Research Square

Preprints are preliminary reports that have not undergone peer review.
They should not be considered conclusive, used to inform clinical practice,
or referenced by the media as validated information.

Strength of sand in plane strain conditions: insights from legacy experimental data

Jos de Greef

jos.de.greef@witteveenbos.com

Henri John Lengkeek
Vahid Galavi

Research Article

Keywords: plane strain, friction angle, shear band, localization, sand

Posted Date: September 19th, 2025

DOI: https://doi.org/10.21203/rs.3.rs-7648179/v1

License: This work is licensed under a Creative Commons Attribution 4.0 International License.
Read Full License

Additional Declarations: The authors declare no competing interests.

Strength of sand in plane strain conditions: insights from legacy experimental data

Jos de Greef jos.de.greef@witteveenbos.com

Henri John Lengkeek arny.lengkeek@witteveenbos.com

Vahid Galavi vahid.galavi@witteveenbos.com

Witteveen+Bos Engineering Consultants

ABSTRACT

The plane strain assumption is widely used in geotechnical engineering for boundary value problems such as retaining structures and embankments. In practice, the peak friction angle of cohesionless soils under plane strain conditions is frequently approximated by increasing the friction angle obtained from triaxial compression tests by a factor 9/8 to account for the experimentally observed strength surplus.

This paper demonstrates, both theoretically and experimentally, that this factor is neither constant nor consistently conservative. Using a comprehensive database of legacy experiments -including both independent stress control and plane strain tests, with matching triaxial compression data- a multi-linear regression analysis is performed to identify key predictors of the plane strain strength surplus. In addition to relative density and confining stress, two geometric parameters are significant: (i) the ratio of sample height to the height for a shear band to freely develop across the sample, and (ii) the ratio of sample height to sample length (distance between the zero strain boundaries).

Based on these findings, two empirical relations are proposed for estimating the plane strain strength surplus as a function of relative density and confining stress, conditioned on typical sample geometries: one for uniform strain conditions and one for localized strain conditions. A case study on slope stability demonstrates that the effect of selecting either of these empirical relations on the calculated factor of safety is comparable to (in)adequately capturing localized strain behavior in the model environment. This highlights that the appropriate plane strain strength surplus depends both on soil state and the model's capacity to capture localized strain behavior.

KEYWORDS: plane strain, friction angle, shear band, localization, sand

LIST OF SYMBOLS AND ABBREVIATIONS

b	Intermediate principal stress parameter
β	Shear band orientation relative to σ_3
CI	Confidence interval
d_{10}	Effective grain size, 10^{th} percentile from sieve analysis
d_{50}	Median grain size diameter, 50^{th} percentile from sieve analysis
d_{60}	60^{th} percentile from sieve analysis
e	Void ratio
e_{min}	Minimum void ratio
e_{max}	Maximum void ratio
D_R	Relative density
$D_{R;c}$	Relative density after consolidation
$D_{R;i}$	Initial relative density
f1	Failure condition defined at $(\sigma_1-\sigma_3)_{max}$
f2	Failure condition defined at $(\sigma_1/\sigma_3)_{max}$
FE(M)	Finite Element (method)
FoS	Factor of safety (referring to slope stability)
φ	Friction angle
H	Height of a cuboidal sample
H_{SB}	(Estimated) height for a shear band to freely develop
L	Length of cuboidal sample
LD	Lade-Duncan
LE(M)	Limit Equilibrium (method)
MC	Mohr-Coulomb
MLR	Multi-linear regression
MN	Matsuoka-Nakai
p_a	atmospheric pressure = 101.3 kPa
PS	Plane strain (compression)
n	Porosity
N	Number of experiments / data points (generic)
r	Ratio between $\varphi_{b>0}/\varphi_{b=0}$ ($=\varphi_{ps}/\varphi_{tc}$ in plane strain)
σ	(Effective) normal stress
σ_1	Major principal (effective) stress
σ_2	Intermediate principal (effective) stress
σ_3	Minor principal (effective) stress
TC	Triaxial compression
τ	(Critical) shear strength
UC	Uniformity coefficient = d_{60}/d_{10}
W	Width of a cuboidal sample
ξ	Angle between the rotation plane of ω and the plane strain boundary
ψ	Dilatancy angle
ω	Angle between the deposition direction and the principal (effective) stress

subscripts

p	referring to peak condition in experiments
c	referring to critical (or constant volume) condition in experiments
tc, b=0	referring to triaxial compression experiments
ps	referring to plane strain experiments
b>0	referring to independent stress control and plane strain experiments
f1	referring to failure condition f1 in undrained experiments
f2	referring to failure condition f2 in undrained experiments
k	characteristic

1. INTRODUCTION

Most boundary value problems in geotechnical engineering are analyzed under the assumption of plane strain (PS) condition, such as retaining structures and embankments. This assumption is valid provided that the variations in geometry and material properties are negligible in the out-of-plane direction.

It is widely observed that under laboratory conditions, the measured peak friction angle (denoted φ_p) of cohesionless soils in plane strain compression $\varphi_{p;ps}$ is higher than in triaxial compression $\varphi_{p;tc}$. This observation has been reported in numerous experimental studies, conducted by different researchers, on various types of sand, and using different experimental techniques.

For modelling purposes, the Mohr-Coulomb (MC) yield criterion is typically used to describe yielding behavior of granular soils. In the MC model, the friction angle φ is expressed solely as a function of the major and minor principal stresses, σ_1 and σ_3 respectively, as shown in Eq. 1. However, the experimental tests show that the peak friction angle φ_p is a function of the intermediate principal stress σ_2 as well, generally increasing as $\sigma_2>\sigma_3$.

$$\sin\varphi = \frac{\sigma_1 - \sigma_3}{\sigma_1 + \sigma_3} \qquad \text{Eq. 1}$$

In engineering practice, there is no consensus on how to account for the fact that, in general, $\varphi_{p;ps}>\varphi_{p;tc}$. Within finite element (FE) environments, it is possible to adopt a yield surface alternative to MC that depends on all three principal stresses. Alternatively, the MC yield criterion may be retained, while applying a higher equivalent friction angle such that the ratio σ_1/σ_3 at failure matches that obtained with a more advanced yield surface [37]. The latter approach allows to apply a strength surplus outside of FE environments too, such as limit equilibrium methods (LEM) or code-based spreadsheets calculations.

Several design codes and guidelines incorporate adjustment of the friction angle to account for plane strain conditions. Since 2017, the Dutch National Annex to Eurocode 7 [69] allows a factor of 9/8 on the friction angle for plane strain finite element analyses, provided the friction angle is based on triaxial compression (TC) test results. This factor closely matches the relation $\varphi_{p;ps} = 1.12\cdot\varphi_{p;tc}$, reported for cohesionless soil [49]. The EAU recommendations for waterfront structures [29] also adopts the factor of 9/8 but states that a surplus 10% can only be applied to dense sands. The guideline CIRIA C580 on the design of embedded retaining walls [19] notes that the critical friction angle in plane strain $\varphi_{c;ps}$ is about 10% higher than the critical friction angle in triaxial compression $\varphi_{c;tc}$ while referring to the work by [99]. However, an opposite observation is reported in [99], namely that *there is some evidence to suggest that for a given material φ_c in plane strain is a little higher than for triaxial loading* but that *the conservative estimate is made here they are the same*. Lastly, in the Danish National Annex to Eurocode 7 [94] in relation to the bearing resistance of spread foundations the relation $\varphi_{p;ps}=(1+0.1\cdot D_R)\varphi_{p;tc}$ is used where D_R denotes the relative density of the granular soil.

The factor 9/8, presented as a fraction in Dutch National Annex [69] and EAU [29] originates from [118], where it was derived as an engineering approximation based on the Matsuoka-Nakai (MN) yield criterion [63] under the assumption of an associated flow rule. The MN yield criterion was selected in [118] for several reasons, one being that it provides the best fit to available experimental data.

Previously aggregated experimental data comparing $\varphi_{p;ps}$ and $\varphi_{p;tc}$ [34,91] show that the ratio $\varphi_{p;ps}/\varphi_{p;tc}$ is not constant but varies with $\varphi_{p;tc}$ (and, indirectly, with D_R as follows from [94]). These data indicates that a fixed factor of 9/8 is unconservative, particularly at low values of $\varphi_{p;tc}$. Ideally, each data point in a $\varphi_{p;ps}$ versus $\varphi_{p;tc}$ comparison should be derived from paired tests performed on the same sand with identical density and confining pressure, and identical laboratory conditions (i.e. by the same technician at approximately the same time). Upon closer inspection of the published data it is found that often one or more of these conditions is not met, and some of the presented data points could not be reproduced.

Since the 1960s onwards multiple studies have been published concerning independent stress control (ISC) tests using other apparatuses than plane strain tests, such as cuboidal true triaxial and hollow cylinder devices. These tests enabled assessment of soil strength under general stress conditions and has resulted in development of yield surfaces alternative to MC, such as Lade-Duncan (LD) [51] and MN [63], which in contrast to MC depend on the

value of the intermediate principal stress σ_2. The value of σ_2 relative to σ_1 and σ_3 can be expressed through the parameter b (Eq. 2) or equivalently by the Lode angle θ. In this paper, the parameter b is used:

$$b = \frac{\sigma_2 - \sigma_3}{\sigma_1 - \sigma_3} = \frac{1}{2} - \frac{\sqrt{3}}{2}\tan\theta \qquad \text{Eq. 2}$$

The shape of the LD and MN yield surfaces is governed by the friction angle in triaxial compression φ_{tc} using Eq. 1. Their variation with φ_{tc} is presented in Fig. 1, where r is plotted as a function of b for different values of φ_{tc}. Here, r is defined as the ratio of $\varphi_{b>0}/\varphi_{b=0}$, which in the case of plane strain tests is equivalent to $\varphi_{ps}/\varphi_{tc}$. Note that the MC criterion could be represented in Fig. 1 by a horizontal line at r=1.

Referring to previous experimental data [74], the value of b at failure in plane strain conditions is reported to range approximately between b=0.10 and b=0.50, and [56] approximates its value in tests as b=0.30. Fig. 1 shows that for these values of b, the difference in r between LD and MN is significant. While both yield surfaces are supported by experimental evidence by the respective authors, it is not evident a priori which contour provides the best performance in FE boundary value problems, either in terms of failure prediction or deformation behavior.

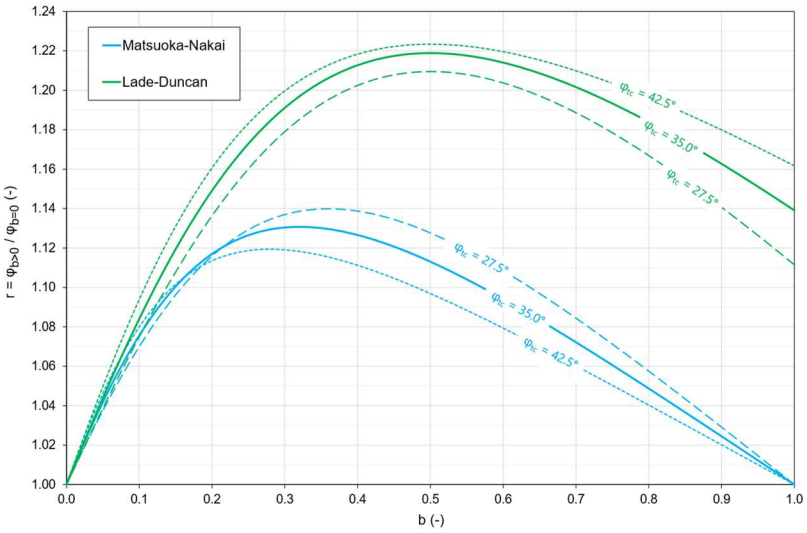


Fig. 1: Strength surplus r as a function of b for the LD and MN yield criteria for different values of φ_{tc}

In addition to the shape of the yield surface, Fig. 1 shows that the value of r is a function of b. Under the assumption of associativity adopted in [118], the value of b for the MN criterion in plane strain is exactly the value at which r is maximum [38,89]. As shown in Fig. 1, varying φ_{tc} demonstrates that the factor 9/8 is not a constant, even if the assumptions of [118] hold. It is approached only at φ_{tc}=39.0°, where r=1.125 (at b=0.30).

In FE analyses the value of b in plane strain is determined by the plastic potential function, g, that governs the direction of plastic strains [73]. For granular soils, the dilatancy angle ψ is generally smaller than φ, and therefore, the plastic potential g differs from the yield function f. Hence, granular soils are generally non-associative.

Both assumptions of [118] underlying the factor 9/8, namely the appropriateness of the MN yield surface and associative behavior, are therefore debatable. Moreover, even under these assumptions, it is shown that the factor is not a constant. For engineering purposes it is important to know how, and to what extent, these factors affect the plane strain strength surplus, both from experimental evidence, and practical implementation in modeling environments.

The goals of this paper are threefold. First, in section 2 it is explained in an accessible manner what factors govern the plane strain strength. Second, the plane strain strength surplus is quantified by compiling a legacy experimental database of both PS and ISC tests on sand, and the effect of the discussed governing factors is examined. The methodology, used to establish the database and combine the experimental data, are described in section 3, and results are presented in section 4. Third, these findings are translated into engineering practice, specifically

regarding the application of a plain strain strength surplus (section 5). The conclusions are summarized in section 6.

Conventions

Throughout this paper, the soil mechanics sign convention is adopted, i.e. compressive stresses are taken as positive. All stresses refer to effective stresses unless stated otherwise. Therefore, the apostrophe is omitted. The relative density of granular soil is denoted by D_R. In earlier publications, porosity, n, or void ratio, e, were used as measures of density. In such case, values were converted to $D_R=(e_{max}-e)/(e_{max}-e_{min})$ by taking the reported limiting porosities (or void ratios e). It should be noted, however, that some studies did not report the limiting porosities [47,119].

In the remainder of this paper, it is sometimes referred to what is *common practice* in geotechnical engineering. It is fully acknowledged that this is a subjective notion as it strongly depends on the experience and expertise of the geotechnical engineer. It is based on daily observation in practice, both within an engineering firm and through collaboration, peer review and published literature.

2. FACTORS AFFECTING PEAK STRENGTH IN PLANE STRAIN

In assembling a legacy experimental database and evaluating the data, this section highlights some of the factors influencing the measured value of $\varphi_{p;ps}$ and consequently the surplus relative to $\varphi_{p;tc}$.

To set a framework, the method by Lade [55] is used, who addresses the inconsistency in published experimental data from legacy ISC tests by categorizing the behavior of φ_p as a function of b in 3 distinct groups. The behavior of these groups is schematically illustrated in Fig. 2. Group 1 shows a continuous increase of φ_p as b increases from 0 to a value of ~0.5-0.8 and a slight decrease as b approaches 1. In general $\varphi_{p;te}>\varphi_{p;tc}$. Group 2 shows behavior similar to group 1 near b=0 and b=1, but the increase of φ_p in the midrange of b values is suppressed. Group 3 shows an increase of φ_p as b increases from 0 to ~0.4, but φ_p decreases with further increasing b, with $\varphi_{p;te}\approx\varphi_{p;tc}$.

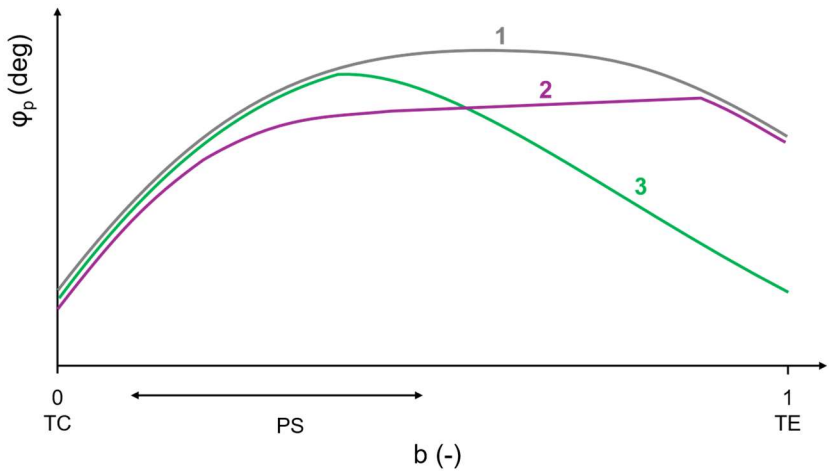


Fig. 2: Typical behavior of φ_p as a function of b for groups 1, 2 and 3 as defined in [55]

The difference between groups 1 and 2 is due to the occurrence of localized strains within shear bands during the hardening regime of the tests in group 2. The strain localization suppresses the strength that would be achieved under uniform strain conditions as observed in group 1. The difference between group 3 and the other two groups can be explained by cross-anisotropy of the sample. At failure in triaxial extension, σ_1 is perpendicular to the bedding plane in groups 1 and 2, whereas in group 3, σ_1 is parallel to the bedding plane. This means failure occurs in a different sector of the deviatoric plane. On this basis, [55] suggested that the experimental evidence to support MN is in that sense flawed. However, some experimental observations remain that cannot be explained using the original LD yield formulation either [51,52].

For shear banding, [54] proposed a normalized hardening modulus to explain a posteriori the suppression in the midrange of b-values in group 2. To address cross-anisotropy, [2] introduced an extended formulation of the LD yield criterion. For the assessment of the experimental data in this study, the question of whether $\varphi_{p;te}$ is generally equal to or higher than $\varphi_{p;tc}$ is of limited relevance as the focus lies on plane strain conditions. However, in determining and aggregating the values of r_p and aggregation of the data, it is important to distinguish between the different sectors of the octahedral plane (Fig. 8).

2.1 Factors affecting strength in triaxial compression

Based on [7], it is clear that $\varphi_{p;tc}$ from drained triaxial tests is strongly influenced by relative density D_R and confining pressure σ_3. A similar dependency on initial relative density and confining pressure is observed for the constant volume friction angle $\varphi_{cv;tc}$, although the (axial) strain level and dilation rates of this data are not provided. This observation appears contradictory to the concept of a unique critical state friction angle φ_c, as proposed in [14]. Often in the literature, φ_{cv} and φ_c are considered to be the same [91] although [45] argue that φ_c should be used to refer to the critical state, rather than the possible quasi-steady state.

Assuming φ_c is indeed a constant, [17] presents some guidance on the factors affecting its values: φ_c increases with increasing particle angularity and decreases with increasing uniformity. To obtain the peak friction angle, a dilation term is added in [17] as a function of D_R. The dilation term is valid for siliceous sands and gravels reaching failure at mean effective stresses up to 400 kPa. Beyond this stress level, suppression of dilation is observed [6]. At high stress levels, crushability of the particles and thereby mineralogy become factors to take into account.

It is assumed implicitly by [14] and explicitly by [91] that φ_c is independent of test configuration, i.e. $\varphi_{c;tc}=\varphi_{c;ps}$. Experimental evidence for this assumption is provided by [20,21], who performed strain-controlled TC and PS tests across a wide range of relative densities. A constant volume friction angle of ~32° is obtained both from the post peak behavior under near constant volume conditions, and by extrapolating the D_R-φ_p trend for triaxial and plane strain data to $D_R \approx 0\%$. Here, the importance of the assumption of constant φ_c in light of the discussed methods is emphasized to account for a larger plane strain surplus. If the MN yield surface is adopted in a FE environment (e.g. using [33]), the relative surplus is in fact largest at low values of φ_{tc}, consistent with the trend shown in Fig. 1.

Undrained tests on sands are typically performed at (very) low relative densities, often to investigate the liquefaction susceptibility. For $D_R>20\%$, it has been shown by [7] that both D_R and σ_3 affect the friction angles obtained from undrained triaxial tests at a shear strain of 6%. Around $D_R=20\%$ the friction angle from undrained triaxial tests approaches $\varphi_{c;tc}$ from drained tests and although it increases with increasing relative density, it remains significantly lower than $\varphi_{p;tc}$ from drained tests.

Instead of presenting results at a specified shear strain level, most studies present the results of undrained tests at the condition of maximum deviatoric stress or maximum stress obliquity. Here, for undrained tests, the following notations are used: Condition f1: $(\sigma_1-\sigma_3)_{max}$ with friction angle φ_{f1}; Condition f2: $(\sigma_1/\sigma_3)_{max}$ with friction angle φ_{f2}. In addition, some studies [31] report results at the quasi-steady state for some tests. This condition is not addressed in present study.

2.2 Sample geometry

Most of the ISC tests considered in this study and all of the PS tests are performed on cuboidal samples with varying dimensions. The only exceptions are the ISC tests performed with the hollow cylinder (HC) and hollow cylinder torsional (HCT) apparatuses [102,119]. Therefore, only cuboidal sample dimensions are discussed here. The height of a cuboidal PS sample is designated by H, the width by W, and the length by L. The alignment of these dimensions with the principal stress directions is visualized in Fig. 3.

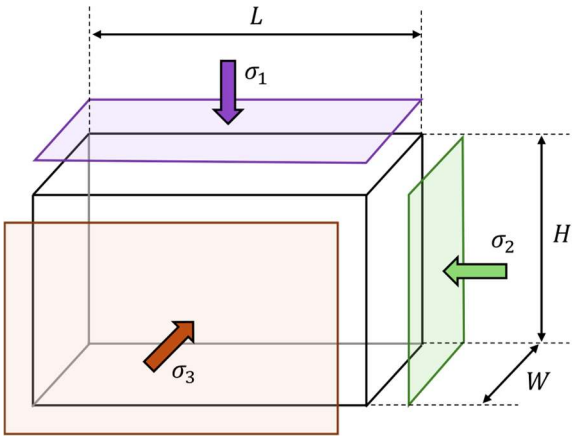


Figure 3: Definition of height (H), width (W) and length (L) of a cuboidal sample

2.3 Shear bands

In this section the effects of shear bands on experimental and numerical plane strain results are discussed. The main purpose is to demonstrate, from an engineering perspective, how shear bands may affect the results in both experimental and model environments. The presented fictive case study and model results serve as a basis for the discussion in section 5.3.

Effect of shear banding on plane strain test results

Shear band formation causes localization of strains in narrow bands. The behavior at the shear band can dominate the overall behavior of the sample, but its effect is captured only indirectly through measurement of the principal stresses σ_1 and σ_3 at the sample boundaries. When considering peak strengths, shear banding is particularly relevant as it can suppress the maximum (effective) stress ratio σ_1/σ_3 that would have been achieved without the shear band. In [54], a posteriori explanation of the suppressed strength for midrange of b-values was found by calculating a normalized hardening modulus just prior to shear band development. Several parametric studies have investigated

the predicted occurrence of shear bands as a function of b, considering different (combinations of) yield surfaces and plastic potentials [65,72,86,87,106,108]. For the purpose of comparing triaxial and plane strain tests, these studies are in qualitative agreement in the sense that shear banding is more likely to occur in plane strain tests and, unlike triaxial compression tests, it can occur within the hardening regime. A simplified visualization based on the Mohr-Coulomb model [109] is presented in Fig. 4 to exemplify the difference between uniform and localized strains.

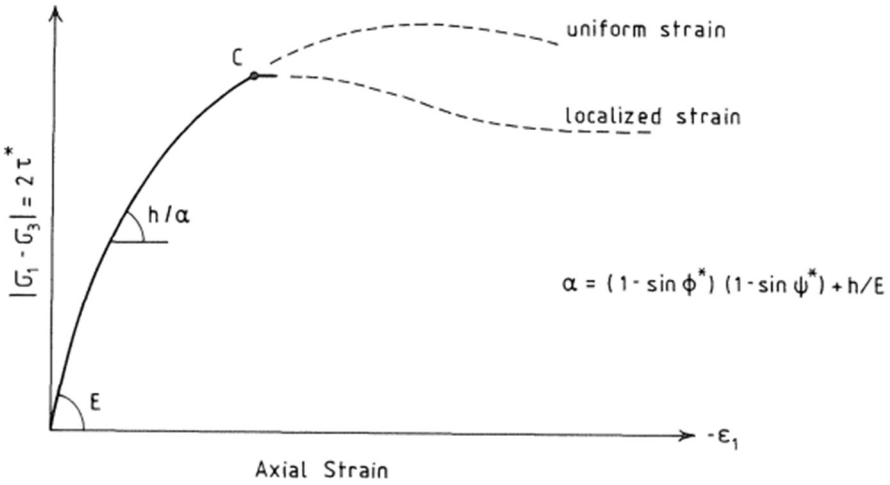


Fig 4: Possible post-bifurcation response (from: [109]) indicating the difference between uniform and localized strain in biaxial conditions

Several factors influence the occurrence of shear bands in ISC and PS tests such as the slenderness of the sample, the grain size relative to the sample dimensions and the sample boundaries (and applied lubrication at these boundaries) [55]. Regarding these factors, the principle question is whether shear bands can freely develop.

A schematic PS test configuration is shown in Fig. 5 from the viewpoint of the σ_2 direction where β represents the shear band orientation relative to σ_3. The Roscoe [82] and Coulomb [22] orientations define the theoretical limits of β under biaxial loading conditions [110]. Although theoretical considerations suggest that shear banding may occur in the hardening regime of a PS test, it is obvious from Fig. 5 that if the ratio H/W is sufficiently low, the shear band will intersect with the cap or base of the specimen, irrespective of its precise orientation. The width of a shear band depends on median grain size diameter d_{50} [26,67] and is typically around $15d_{50}$ [110]. Larger grain size diameters result in wider shear bands and therefore are more likely to be influenced, or even prevented from forming, by the cap and base of the sample. At low H/W ratios, well-lubricated cap and base surfaces are expected to further enhance uniform strains [53,55,88]. In this paper the effect of lubrication on the results is not considered, as it is difficult to quantify the effect of certain lubrication types, if at all specified in the literature.

Here, the required height for a shear band to freely develop, H_{SB}, is evaluated relative to the height of the sample H, denoted as H/H_{SB}. As shown in Fig. 5, the value of H_{SB} is estimated as the summation of the height of a fully developed shear band in the sample, $W\tan\beta$, and the vertically projected width of the shear band, $15d_{50}/\cos\beta$. The angle β is estimated as the intermediate orientation of the Roscoe and Coulomb bounds, i.e. $\beta=45°+(\varphi+\psi)/4$ [9]. Here, the measured peak friction angle, φ_p, is applied and the relation $\psi=(\varphi_p-\varphi_c)/0.8$ [14] is used. For simplicity, φ_c is considered to be 30°, irrespective of the type of sand.

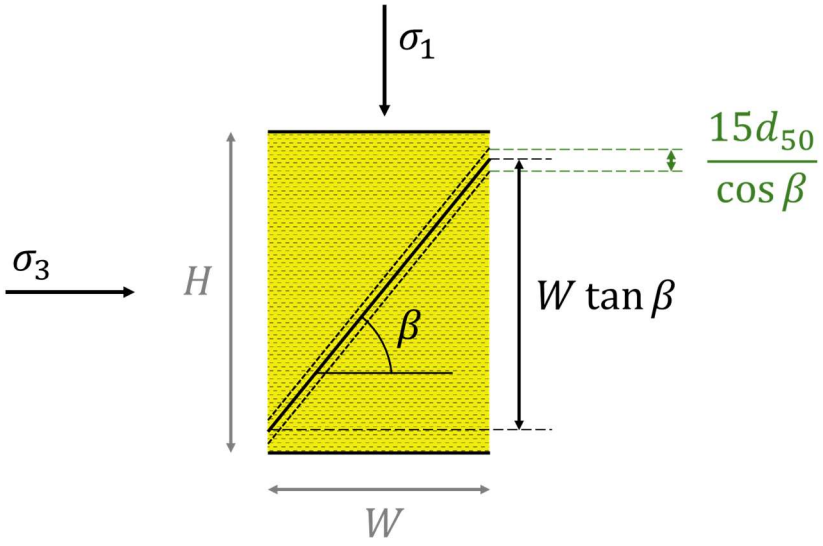


Fig. 5: Schematic side view of a plane strain test (from the σ_2 direction)

For most of the experimental data in groups 1 and 2 reported by [55], the type of sand, height, width and median grain size are presented in Table 1, together with the corresponding ratios H/W and H/H_{SB}. In all cases $H<H_{SB}$, implying that a shear band does not necessarily has to traverse the sample, as depicted in Fig. 5, to suppress the measured strength. Apart from the Ham River sands, with clearly higher H/W and H/H_{SB} ratios, there appears to be no clear distinction between groups 1 and 2 in terms of these ratios. In anticipation of the results presented in section 4.2, the ratio H/H_{SB} proves to be a significant predictor of r_p when all data, including PS test data, is evaluated.

Table 1: Comparison of median grain size diameter, H/W ratio and H/H_{SB} ratio for group 1 (uniform strain) and group 2 (localized strain) by [55]

	ref	sand	H [mm]	W [mm]	d_{50} [mm]	H/W [-]	H/H_{SB} [-]
Group 1 (uniform)	[47]	Ottawa_1 (med dense)	93.4	93.4	0.6	1	0.46
		Ottawa_1 (med loose)	93.4	93.4	0.6	1	0.56
	[9]	Leighton Buzzard	100	100	0.725[1]	1	0.46
	[70]	Cambria	76	76	1.42[1]	1	0.40
	[120]	Fuji River	100	100	0.4	1	0.51
Group 2 (localized)	[50]	Monterey_0 (dense)	76	76	0.43	1	0.38
		Monterey_0 (loose)	76	76	0.43	1	0.54
	[75]	River Welland[2]	120.7	120.7	0.128[2]	1	0.48
	[81]	Ham River_1	84	53	0.285	1.58	0.89
	[35]	Ham River[3]	83.8	53.3	0.239[3]	1.57	0.85

[1]average of reported maximum and minimum sieve sizes

[2]not included in the database of this study, as it could not be established whether the data was unique compared to the data from [46] and [117]. The value of d_{50} is assumed to be equal to these studies

[3]not included in the database of this study, as the results reported by [81] were considered to supersede them. The value of d_{50} could be derived from the grain size distributions provided in [81], using the average value of 2 batches with d_{50} equal to 0.219 and 0.259 mm

Effect of shear banding on FE results

In plane strain finite element analyses, the occurrence, orientation and thickness of shear bands are generally mesh dependent for non-associative materials [106]. Based on the early findings of [23], it is often believed that the effect of ψ, and thus the degree of non-associativity, on failure loads is minor for kinematically unconstrained problems [97]. According to [41], slope stability is an unconstrained problem, while referring to numerical simulations by [121], in which the effect of varying dilation angle on the factor of safety is assessed for a simple

homogenous slope. In these simulations, approximately 76 elements of 2.5 x 2.5 m were used, each containing 4 Gauss points, corresponding to an average number of 0.64 Gauss points per m^2.

A parametric study by [92] presents and discussed the application of limit equilibrium methods, finite element limit analysis and the strength reduction procedure in FE for slope stability problems. One of the fictive case studies reported therein is adopted here. It is a 20 m high slope with an inclination of 35° (1:1.43) consisting of homogeneous dry material with φ=35° and c=5 kPa. The results presented in Table 2 are obtained using the strength reduction procedure implemented in Plaxis 2D [12], adopting the standard Mohr-Coulomb constitutive model. No local mesh refinements are made.

Table 2: Calculated factor of safety (FoS) obtained using the FE strength reduction procedure for a simple slope with different mesh densities and dilatancy angles ψ

elements	Gauss points per m^2	FoS (ψ=0°)	FoS (ψ=6.3°)	FoS (ψ=35°)
118	0.45	1.238	1.262	1.289
203	0.78	1.212	1.244	1.291
1828	7	1.159	1.207	1.273
78085	301	1.101	1.166	1.275

The results for ψ=0° and ψ=35° correspond well to those reported in [92]. Even with a similar number of Gauss points per m^2 as in [121], a clear influence of ψ on FoS is observed. The mesh dependency continues beyond what is usually considered to be a sufficiently fine mesh in practice (1828 elements). This effect is most evident as ψ approaches 0°, which is in agreement with the findings of [92]. The case of ψ=6.3° is included as an approximation of dilation angle, typically calculated for φ_p=35° using the relation given by [14].

The results for the two finest meshes from Table 2 at ψ=0° are visualized in Fig. 6, which shows the values of the parameter b in the cross-section. It is observed that a finer mesh results in a narrower shear band, with slightly higher b values in the shear band. However, in both cases the values of b remain lower than what is typically found in PS tests or in pure shear (b=0.5). This find is in qualitive agreement with [107], which reported that, when a Mohr-Coulomb type of plastic potential is adopted, the stress paths near the triaxial compression points tend to converge towards the triaxial compression point, which results to an underestimation of b values.

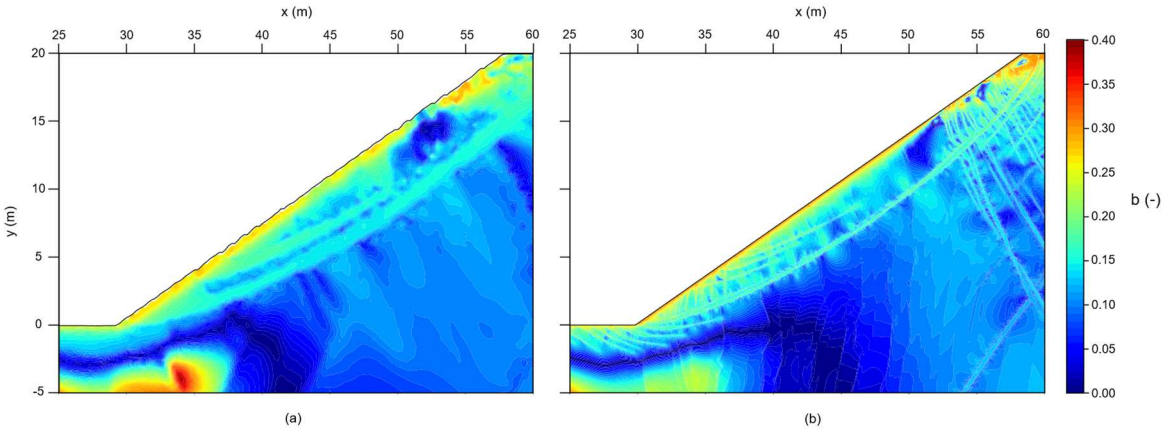


Fig. 6: Shape of shear bands and b values for the fictive case study at ψ=0°: (a) at 7 Gauss points per m^2, (b) at 301 Gauss points per m^2

Effect of shear banding on LE results

To obtain analytical or limit equilibrium solutions, the shear band orientation β must be determined a priori to assess the shear capacity of the soil. As demonstrated by [105], the Coulomb orientation (β=45°+φ/2) results in the traditional Mohr-Coulomb expression τ=σ·tan(φ) irrespective of the value of ψ, whereas the Roscoe orientation (β=45°+ψ/2) results in the Davis expression [23], which simplifies to τ=σ·sin(φ) at ψ=0°. An alternative suggestion by [9] is β=45°+(φ+ψ)/4 which has been experimentally validated. This orientation will be named the Arthur orientation after the first author. Irrespective of whether β is expressed as a function of φ, ψ, or both, the ratio τ/σ can be derived as a function of φ and β directly through Eq. 3.

$\frac{\tau}{\sigma} = \frac{(R-1)\cos(2\beta - 90°)}{R-(R-1)\sin(2\beta-90°)+1}$	$R = \tan^2(45° + \varphi/2)$	Eq. 3

The fictive slope, considered in the FE simulations, is also analyzed here using LE calculations with the Bishop and Spencer algorithms, as implemented in D-Stability [24]. The effect of β on the calculated FoS is presented in Table 3 for some of the orientations discussed above. Although in D-Stability it is possible to independently provide φ and ψ as input in the Davis expression, the Roscoe orientation is still assumed implicitly. Therefore an equivalent friction angle φ* and cohesion c* are determined through Eq. 4. For the Roscoe orientation these expressions are equivalent to the Davis expression. In the last row of Table 3 the value of β is determined iteratively, such that the LE results match the FE results in Table 2 for the finest mesh considered.

$\varphi^* = \tan^{-1}\left[(\tau/\sigma)_\beta\right]$	$c^* = c \cdot \frac{(\tau/\sigma)_\beta}{(\tau/\sigma)_{\beta=45°+\varphi/2}}$	Eq. 4

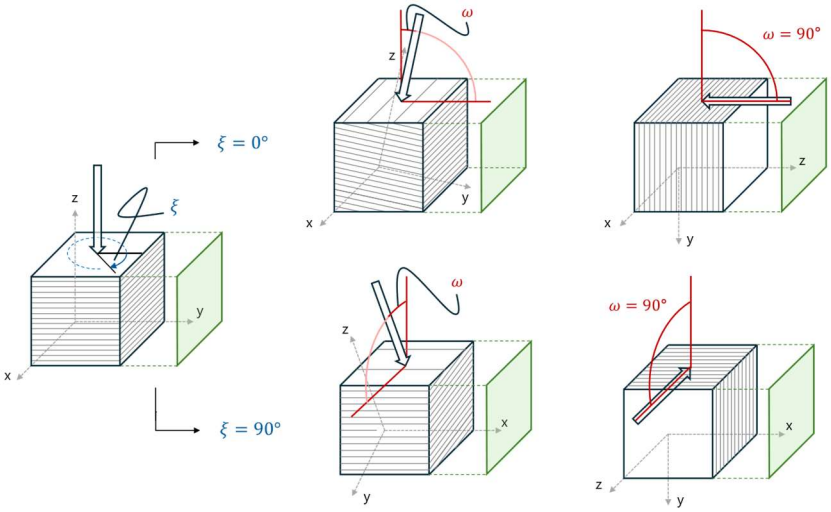
Table 3: Calculated factor of safety (FoS) from LEM slip circle analysis of a simple slope for different shear band orientations β at ψ=0° and ψ=10°

		ψ=0°		ψ=6.3°	
Orientation	**equation for β**	**β [°]**	**FoS [-] (Spencer / Bishop)**	**β [°]**	**FoS [-] (Spencer / Bishop)**
Roscoe [82]	45°+ψ/2	45.0	1.049 / 1.048	48.1	1.111 / 1.111
Coulomb [22]	45°+φ/2	62.5	1.279 / 1.279	62.5	1.279 / 1.279
Arthur [9]	45°+(φ+ψ)/4	53.8	1.207 / 1.208	55.3	1.229 / 1.229
best fit to finest mesh in FEM		47.6	1.101 / 1.100	51.1	1.166 / 1.165

From Table 3 it can be observed that the Roscoe orientation yields more conservative results than the finest FE mesh considered, but still provides a better approximation than either the Coulomb or Arthur orientations. Findings reported in [10] indicate that the shear band orientation is related to the coarseness of the material, or at least the coarseness compared to the membrane thickness [110]. However, a more rigorous experimental study by [111] shows that mean grain size cannot be directly related to shear band orientation. The present paper does not address the shear band orientations observed experimentally in (some of the) tests.

2.4 Principal stress orientation and inherent anisotropy

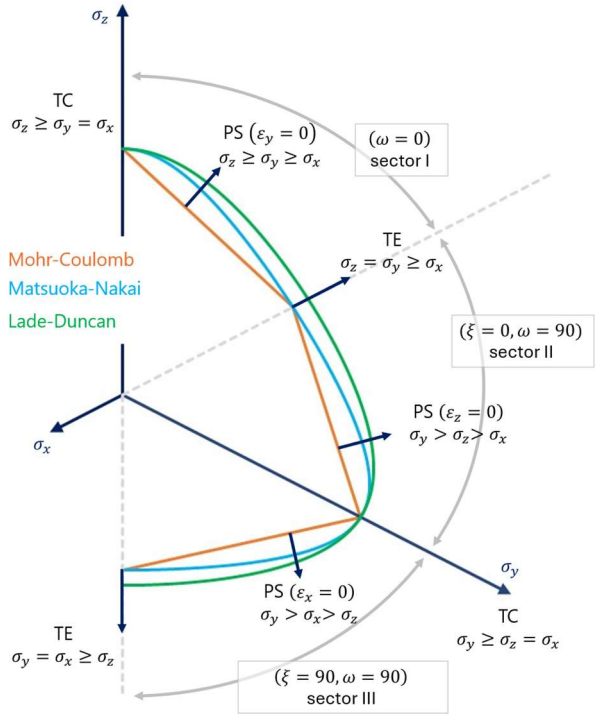
Most yield surfaces commonly adopted in engineering practice are defined isotropically. Experimental results, however, show clear effects of fabric [57] and inherent anisotropy [8]. In particular, the orientation of the principal stresses relative to the bedding plane has an influence on the observed stress-strain behavior. Different nomenclatures exist to express this orientation, but in present paper the convention by [57] is adopted, as visualized in Fig. 7. The x, y and z axes correspond to the σ_1, σ_2 and σ_3 directions, respectively, in a standard plane strain compression test. The angle ω depicts the angle between the deposition direction (perpendicular to the bedding plane) and σ_1 during the test. The angle ξ depicts the rotation between the plane, in which ω rotates and the plane strain boundary - depicted in Fig. 7 by the green surfaces in accordance with Fig. 3. It is obvious that when ω=0°, the value of ξ is irrelevant.



353

354 Fig. 7: Bedding plane orientations relative to principal stress directions

355 Alternatively, anisotropy can be depicted by referring to the sectors in the octahedral plane. Plane strain
356 compression tests at ω=0° correspond to sector 1, tests at (ξ=0°, ω=90°) correspond to sector 2, and tests at (ξ=90°,
357 ω=90°) correspond to sector 3. The different sectors of the octahedral plane are presented in Fig. 8, including a
358 visualization of the MC, MN and LD yield surfaces.



359

360 Fig. 8: Sectors in the octahedral plane

3. METHODOLOGY

3.1 Data acquisition

Experimental data is obtained from multiple sources, mainly being journal publications, conference papers and PhD dissertations available through university repositories. In most PS tests, the peak strength at a set or wide range of relative densities was considered. Depending on the goal of the study, confining stress level, sample dimensions, bedding planning orientation, or combinations of these factors were varied. In studies concerning ISC tests, the value of b was varied on samples with (nearly) equal relative density. Additional variations in these studies were limited mainly to the consideration of inherent anisotropy by assessing the strength behavior in the full octahedral plane.

In setting up the database, the same aspects need to be evaluated that are mentioned in section 1 regarding the reproducibility of the $\varphi_{p;ps}$ versus $\varphi_{p;tc}$ plots in [34,91]. For a sensible comparison of TC and PS test results, data should ideally be obtained from the same material, preferably tested by the same laboratory technician (or department) during the same period, adopting similar (ranges) of relative densities and/or confining stresses. While this is explicit in some studies, in other cases, however, the full set of available data is distributed across multiple publications. In these cases, above aspects were evaluated to decide whether to include or exclude the results. In addition, it was carefully checked to avoid duplication of data. The aim in setting up the experimental database was to retrieve the principal stresses and axial strain ε_1 at peak strength, from which the parameters φ_p and b_p can be calculated using Eq. 1 and Eq. 2, respectively.

Experimental results are presented either in tables, figures, or both. If not clearly erroneous, tabulated values are always given precedence. If the test ID is provided, this ID is used in the database. If data is only presented in figures, the test ID is related to the corresponding figure, e.g. Fig6_TC1, Fig6_TC2, etc. Together with the reference listed in the database, this ensures that all data is traceable. Often data is presented in multiple figures that are combined to get the full data per test. In most cases, this is possible, as the relative density, friction angle or axial strains are unambiguously unique. If this is not the case, the data is omitted.

An attempt is made to use originally presented data as much as possible. For example, the comparison between triaxial and plane strain data on Mersey River sand by [85] suggests that 4 tests pairs at equal relative densities are available. However, it is established that actually 9 triaxial tests [84] and 5 plane strain tests [117] are performed, all during the same period at the University of Manchester.

In some studies, membrane and side platen friction corrections are quantified and accounted for, e.g. [61,76,81], while in some other studies corrections are explicitly ignored as they are stated to be negligible, e.g. [21,70]. In most instances, there is no explicit mentioning of the applied corrections. Given this inconsistency, the boundary effects and corrections are not considered in the present study. Therefore, the present study is limited to aggregation of the reported results.

3.2 Data not considered

The authors acknowledge that not all available PS and/or ISC data on sands have been evaluated. Some were not assessed due to the research project constraints [15,40], while others were evaluated but deliberately not included in the database for various reasons as mentioned below.

In [6], four PS tests were performed on Ottawa F-75 sand, and although graphically compared to TC tests, both relative density and confining stress do not match. In [39] multiple PS and TC tests were performed on sands designated as type A, B and C with different relative densities. Multiple issues have been encountered, when interpreting and reproducing the presented results. For instance, the reported typical stress-strain curves could not be matched to any of the tabulated test results. In addition, a near perfect match ($R^2 = 0.997$) has been obtained between the tabulated values of $\varphi_{p;ps}$ at σ_3=172 kPa value, assuming $\sigma_2=2\sigma_3$ and using the empirical expression by [13] for $\varphi_{p;ps}$ by using σ_1, σ_2 and σ_3. There is no obvious reason, why this should be the case, as σ_2 are reported to be measured values. In [96], the results from multiple PS tests on Skarpa sand are presented. Comparative drained TC tests from earlier studies are found [95,101], but the combinations of relative densities and stress levels did not allow for a meaningful comparison between TC and PS tests.

3.3 Database entries

The entries of the compiled experimental database are summarized and briefly described in Table 3. An insightful visual overview of the different types of apparatuses is available in the literature review by [90]. Table 4 lists the apparatuses used in the database, together with their abbreviations, and indicates the type(s) of test performed with each apparatus. A compressed overview of the database is provided in Table 5. For each Sand ID, the database and table includes the basic material properties, the test type, the used apparatuses for b>0 tests along with the dimensions, an indication of whether drained (D) or undrained (U) tests are performed (and the failure condition for the latter), the confining stresses, and relative densities. For these last two parameters, the values of the drained tests are provided in Table 5, if both drained and undrained tests are performed.

Table 3: Database entries

Database entry	**Unit**	**Remarks**
Publication	-	Publication from which the data is obtained
Sand ID	-	Unique name for the sand. For sands with identical names subscripts are used, e.g. Toyoura_1, Toyoura_2, etc.
d_{50}	[mm]	Mean grain size of the sand
e_{min}, e_{max}	[-]	Limiting porosities of the sand
Test ID	-	Unique name for each test, see section 3.1
Apparatus	-	Abbrevation of the employed apparatus for the test, see Table 4
Type of test	-	Abbreviation of the test performed
Drainage	-	Drained or Undrained
Height	[mm]	Sample height
Length	[mm]	See section 2.2 for rectangular test specimens For cylindrical triaxial tests equal to the diameter For hollow cylinder tests equal to the inner diameter
Width	[mm]	See section 2.2 for rectangular test specimens For cylindrical triaxial tests equal to the diameter For hollow cylinder tests equal to the outer diameter
Sector	-	Sector in the octahedral plane, see section 2.4 and Fig. 7
ω, ξ	[°]	Bedding plane orientation, see section 2.4, Fig. 6 and Fig. 7
σ_{1c}, σ_{3c}	[kPa]	Major and minor (effective) principal consolidation stresses
K_0	[-]	Ratio of σ_{3c}/σ_{1c}
e_i	[-]	Initial void ratio (prior to consolidation)
$D_{R;i}$	[-]	Initial relative density (prior to consolidation)
e_c	[-]	Void ratio after consolidation
$D_{R;c}$	[-]	Relative density after consolidation
σ_1,σ_2,σ_3 (f1)	[kPa]	Principal (effective) stresses at $(\sigma_1-\sigma_3)_{max}$
ε_1	[-]	Principal strain at $(\sigma_1-\sigma_3)_{max}$
φ_p,b_p (f1)	[°],[-]	Friction angle and b value at $(\sigma_1-\sigma_3)_{max}$
σ_1,σ_2,σ_3 (f1)	[kPa]	Principal (effective) stresses at $(\sigma_1/\sigma_3)_{max}$
ε_1	[-]	Principal strain at $(\sigma_1/\sigma_3)_{max}$
φ_p,b_p (f1)	[°],[-]	Friction angle and b value at $(\sigma_1/\sigma_3)_{max}$

Table 4: Different types of apparatuses in the database

apparatus	**abbreviation**	**type of test**
true triaxial (cuboidal)	TTX	TC, PS, ISC
triaxial (cylindrical)	TX	TC
plane strain	PS	PS
hollow cylinder torsional	HCT	TC, ISC
hollow cylinder	HC	TC, ISC

3.4 Data aggregation

Depending on the study, the relative density prior to consolidation $D_{R;i}$, relative density after consolidation $D_{R;c}$, or both are reported. To avoid generating two datasets, it is beneficial to convert all data to one metric. By plotting $D_{R;c}$ as a function of $D_{R;i}$ for all experiments where both are available, a clear linear trends emerges as shown in Fig. 9. Using this linear trend, all $D_{R;i}$ data is transformed to $D_{R;c}$ data, if no $D_{R;c}$ data is available. It is noted that the linear relationship holds for all tests in which σ_3<600 kPa. Below this threshold, no clear distinction is found between isotropic and anisotropic consolidation. In the absence of data between σ_3=600-850 kPa, the linear trend no longer holds for σ_3>850 kPa. As particle crushing during consolidation becomes a factor to account for at these confining stresses, the distinction between isotropic and anisotropic consolidation becomes significant. Data to compare $D_{R;i}$ and $D_{R;c}$ at high confining stresses is only available at σ_3=862 kPa (N=16), σ_3=2068 kPa (N=16) and σ_3=2500-3500 kPa (N=12) from 2 studies [3,4]. Trends on these data are used to estimate $D_{R;c}$ for tests on Antioch sand (at σ_3=981 kPa), Hostun sand (at σ_3=800 kPa) and Monterey_20 sand (at σ_3=3447 kPa). For all other tests the linear trend from Fig. 9 is used (if $D_{R;c}$ is not available).

It should be noted that values of $D_{R;i}$ and $D_{R;c}$ in excess of 100% are found. This indicates that the void ratio in tests can be smaller than e_{min} specified according to a certain procedure, e.g. [11]. Likewise, values of $D_{R;c}$, lower than 0% are also found in literature, reflecting that the void ratio in tests can be higher than e_{max}, specified according to a certain procedure, e.g. [48]. Here, differences between procedures to determine minimum and maximum densities of sand are not evaluated.

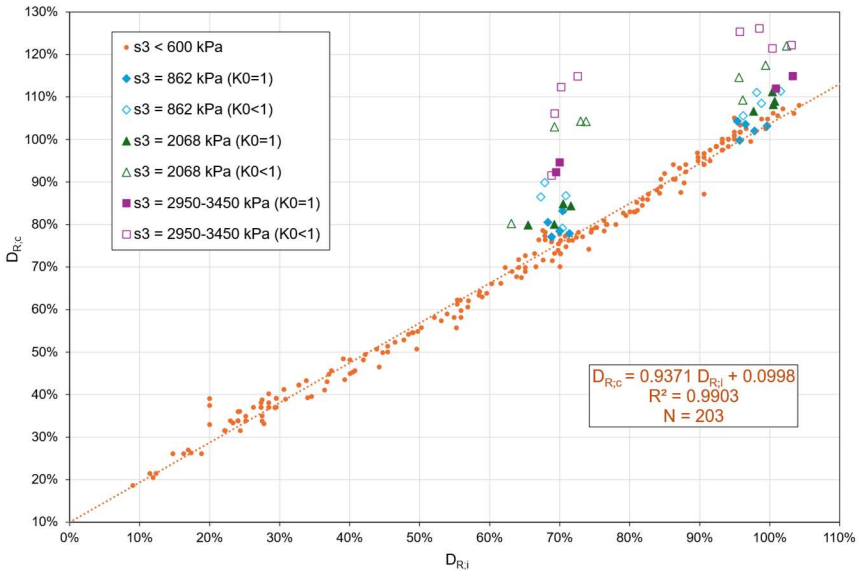


Fig. 9: Comparison of $D_{R;c}$ with $D_{R;i}$ at different consolidation stress conditions

To obtain unbiased r_p values, ideally relative density, confining stress, samples dimensions and bedding plane orientation should be equal. In an attempt to obtain such unbiased r_p values, per study a different approach was used, depending on the applied parameter variations. For ISC tests in a specific sector of the octahedral plane, the value of $\varphi_{p;b>0}$ can simply be compared to $\varphi_{p;b=0}$ which means r_p is determined through pair-wise comparison of the test results. This also applies to some studies, in which PS tests are compared to TC tests at the same relative density and confining stress. For studies, in which a range of relative densities was tested, a regression analysis is applied to the TC data to obtain $\varphi_{p;tc}$ as a function of $D_{R;c}$. In this way, it is possible to determine r_p as the quotient of $\varphi_{p;ps}$ and $\varphi_{p;tc}(D_{R;c;ps})$. Different regressions at different confining stresses are applied, if the results clearly indicate a stress-dependency. This is verified by using multi-linear regression (MLR) analyses. Table 6 gives an overview of the performed regressions and the result in terms of R^2 for the TC tests in the database. The numbers between brackets {} for polynomial regressions refers to the powers included. For example {2,0} means that $\varphi_{p;tc}$ is expressed as $A \cdot D_{R;c}^2 + B$ and the linear term {1} is omitted.

3.5 Data analysis

The aim of the data analysis is primarily to understand and quantify how r_p depends on discussed factors such as relative density, confining stress and sample dimensions. The bulk of the available ISC/PS data concerns drained tests falling in sector 1 of the octahedral plane. This data is used for the statistical analysis. Given the aim to understanding trends, rather than making accurate predictions, this study is limited to simple MLR analysis using complete data. Experimental results from undrained tests and drained tests in sectors 2 and 3 are also presented and discussed, but no thorough data analysis is performed on this data.

459 Table 5: Compressed overview of the compiled experimental database

Sand ID	**Reference(s)**	**d_{50} [mm]**	**e_{min} [-]**	**e_{max} [-]**	**tests**	**appa-ratus**	**H [mm]**	**W [mm]**	**L [mm]**	**D**	**U**	**σ_{3c} [kPa]**	**$D_{R;c}$ [%]**
Antioch	[59]	0.223	0.750	1.140	PS	PS	61	28	71	✓	f1	29-981	45,82,90
Brasted	[20,21]	0.28	0.475	0.792	PS	PS	102	51	406	✓	f2	276	20-87
Cambria	[70]	1.42[1]	0.510	0.800	both	TTX	76	76	76	✓	-	98,196	99
Changi	[114,115,116]	0.30	0.533	0.916	PS	PS	120	60	60	✓	f1	23-300	-14-69
Chattahoochee River	[5]	0.47	0.590	1.090	PS	PS	108	51	406	✓	-	483	51-95
Crushed Napa Basalt	[3]	2	0.535	0.958	PS	PS	114	51	406	✓	-	414-2930	73-126
Ennore	[68]	0.89[1]	0.667	0.923	PS	PS	?	?	?	✓	f1~f2	130-259	78
Fuji River	[120]	0.40	0.480	1.030	ISC	TTX	100	100	100	✓	-	23,24	42,44
Ham River_1	[36,80,81]	0.285	0.613	0.923[4]	both	TTX	84	53	84	✓	-	207	35-103
Ham River_2	[102,103]	0.28	0.613	0.923	ISC	HCT	254	254		✓	-	200	95
Hostun RF	[25,26,27]	0.32	0.626	0.963	PS	PS	335	100	35	✓	-	90-800	39-106
Kobe	[98]	0.34	0.588	0.911	PS	PS	140	40	80	✓	-	100-400	39,88
Leighton Buzzard	[9]	0.725[1]	0.493[5]	0.818[5]	ISC	TTX	100	100	100	✓	-	42	99
Loch Aline	[100]	0.198	0.536	0.802	ISC	TTX	102	102	102	✓	-	138,172	27-88
Masonry	[30,31]	0.32	0.600	0.875	PS	PS	140	40	80	-	f2	159-447	1-8
Mersey River	[84,85,117]	0.235[2]	0.538	0.821[2]	PS	PS	102	102	203	✓	-	34	50-105
Mol	[112]	0.18	0.563	0.887	PS	PS	102	51	406	✓	-	277	51-91
Monterey_0	[50]	0.43	0.565	0.860	both	TTX	76	76	76	✓	-	59	36-105
Monterey_20	[62]	0.55	0.530	0.830	PS	PS	101-292	25-114	114-284	✓	-	69-3447	37-104
Nevada II/ATC silty	[93]	0.12	0.550	0.860	ISC	TTX	76	76	76	✓	-	50	33
Nevada II 50/200	[93]	0.14	0.640	0.880	ISC	TTX	76	76	76	✓	-	50	33
Ottawa_1	[47]	0.6	-	-	ISC	TTX	93	93	93	✓	-	138	?
Ottawa_2	[119]	0.45	-	-	ISC	HC	127	51	76	-	f1+f2	294	?
Ottawa_3	[77,78,79]	0.526	0.471	0.695	both	TTX	76	76	76	✓	-	201	33-95
Painted Rock	[4]	2.05	0.400	0.660	PS	PS	114	51	406	✓	f1	414-2930	77-121
Quartz	[60,61]	0.48	0.429	0.818	PS	PS	600	200	1000	✓	-	98	32-102
River Welland	[46,117]	0.128	0.623	1.004	PS	PS	102	102	203	✓	-	207	49-107
Santa Monica Beach_1	[113]	0.25	0.600	0.910	ISC	TTX	188	76	76	✓	-	49	59,82,97
Santa Monica Beach_2	[1]	0.261	0.570	0.884	ISC	TTX	76	76	76	✓	-	50	97
Skedsmo	[76]	0.224	0.475	0.850	PS	PS	90	35	70	✓	-	4-301	50-55
Sohma sand	[43]	0.599	0.630	0.809	PS	PS	?	?	?	✓	-	?	31,64,93
Toyoura_1	[32,57,58,104]	0.16	0.605	0.977	PS	TTX	55-105	40-55	80-105	✓	-	49,98,392	41-95
Toyoura_2	[42,43]	0.212	0.609	0.990	PS	PS	80	40	320	✓	-	49,98,196[6]	34,54,73,93
Toyoura_3	[71]	0.18	0.630	0.990	PS	PS	60	44	80	✓	-	49,196	98

460

[1]average of reported maximum and minimum sieve sizes

[2]average of reported values by [84] and [117]

[3]estimated from effective grain size (d_{10}) and UC, by using $d_{60} = UC \cdot d_{10}$ and $d_{50} \approx d_{10}+(d_{60}-d_{10})\cdot 4/5$

[4]reported in [103] who adopt the same value

[5]limiting porosities for Leighton Buzzard 18-25 sand taken from [83]

[6]only 4 aggregated TC and 4 aggregated PS data points at different relative densities are included in the database. No designated stress level is included in the database as the reported results in [42] could not be uniquely linked to individual tests. Each data point at a specific relative density represents approximately 9 tests: 3 duplicates at stress levels of 49, 98 and 196 kPa. Data from this study is thereby underrepresented compared to the number of tests actually performed.

Table 6: Overview of the performed TC regression analyses

Sand ID	**Regression**	**R^2**
Antioch	pair-wise (D+U)	-
Brasted	polynomial {2,0} in $D_{R;c}$ (D+U)	0.983 (D) 0.962 (U)
Cambria	ISC, comparison to b=0	-
Changi	polynomial {2,0} in $D_{R;c}$ (D) polynomial {2,1,0} in $D_{R;c}$ at $\sigma_{3c}\approx$150 kPa (U)	0.997 (D) 0.920 (U)
Chattahoochee River	linear in $D_{R;c}$	0.991
Crushed Napa Basalt	linear in $D_{R;c}$ at σ_3=414 kPa linear in $D_{R;c}$ at σ_3=862 kPa linear in $D_{R;c}$ at σ_3=2068 kPa MLR in ($D_{R;c}$; ln(σ_3)) to compare $\sigma_{3;tc}$=3447 kPa with $\sigma_{3;ps}$=2930 kPa	0.977 0.926 0.833 0.968
Ennore	pair-wise, despite some variation in σ_3 between TC and PS (D+U)	-
Fuji River	ISC, comparison to b=0	-
Ham River_1	linear in $D_{R;c}$, MLR showed significance of the H/W ratio, only cuboidal TC tests (H/W=1.45) were included	0.947
Ham River_2	ISC, comparison to b=0	-
Hostun	average from: (a) pair-wise comparison, (b) MLR in ($D_{R;c}$; ln(σ_3)) and (c) linear in $D_{R;c}$ at σ_3=90,300,600 kPa	-
Kobe	pair-wise	-
Leighton Buzzard	ISC, comparison to b=0	-
Loch Aline	ISC, comparison to b=0	-

Masonry	no discernable effect of $D_{R;c}$ (range: 1.5-15.6%), average used	-
Mersey River	polynomial {2,1,0} in $D_{R;c}$	0.989
Mol	polynomial {2,0} in $D_{R;c}$	0.974
Monterey_0	ISC, comparison to b=0	-
Monterey_20	linear in $D_{R;c}$ at σ_3=69 kPa linear in $D_{R;c}$ at σ_3=552 kPa linear in $D_{R;c}$ at σ_3=2068 kPa	0.995 1.000 1.000
Nevada II/ATC silty	ISC, comparison to b=0	-
Nevada II 50/200	ISC, comparison to b=0	-
Ottawa_1	linear in e_i at b=0	0.917
Ottawa_2	only 1 test available at similar stress level and void ratio	-
Ottawa_3	linear in $D_{R;c}$	0.962
Painted Rock dam material	linear in $D_{R;c}$ at σ_3=414 kPa (D) linear in $D_{R;c}$ at σ_3=862 kPa (D) linear in $D_{R;c}$ at σ_3=2068 kPa (D) linear in $D_{R;c}$ at σ_3=2930 kPa (D) pair-wise (U)	0.794 0.967 0.811 0.856 -
Quartz sand	(shifted) polynomial {5,4,3,2,1,0} in $D_{R;c}$	0.998
River Welland	polynomial {2,1,0} in $D_{R;c}$	0.994
Santa Monica Beach_1	ISC, comparison to b=0	-
Santa Monica Beach_2	ISC, comparison to b=0	-
Skedsmo	pair-wise, MLR shows no significance of $D_{R;c}$	-
Sohma sand	pair-wise	-
Toyoura_1	linear in $D_{R;c}$ at σ_3=49 kPa (H/W>2) linear in $D_{R;c}$ at σ_3=98 kPa (H/W>2) polynomial {2,1,0} in $D_{R;c}$ at σ_3=392 kPa (H/W>2) linear in $D_{R;c}$ at σ_3=98 kPa (H/W=1)	0.997 0.979 0.983 0.954
Toyoura_2	pair-wise	-
Toyoura_3	pair-wise	-

471

4. RESULTS

4.1 Typical results

This section presents some typical results of the assembled data. Fig 10a shows, for Brasted sand [20], the measured peak friction angles of both TC and PS tests, and their ratios, r_p, as a function of $D_{R;c}$. The regression trend on TC data, as specified in Table 6, is also shown. The results from the undrained tests are also included. For the undrained PS tests at $D_{R;c}$≈80%, no r_p values are calculated as no corresponding TC tests were available in this range. Fig 10b shows similar results for the tests performed on Toyoura_1 sand [32,57,58,104]. Fig 11a shows, for Cambria sand [70], the measured peak friction angle as a function of b_p for different sectors in the octahedral plane, together with the LD and MN yield surfaces corresponding to $\varphi_{b=0}$. Fig 11b presents similar results for Loch Aline sand [100] evaluated at different values of $D_{R;c}$.

Fig. 12 shows the values of r_p as a function of b_p for all ISC tests and all PS tests, for which b values are available from σ_2 measurements. Fig. 13 shows the major principal strain (axial strain) at failure $\varepsilon_{1;p}$ as a function of $D_{R;c}$ in sector 1 for samples with σ_3<300 kPa. This capping value is somewhat arbitrary, but was chosen as this is a limit that applies to most engineering problems. Over the full range of $D_{R;c}$, the ratio between $\varepsilon_{1;p;ps}$ and $\varepsilon_{1;p;tc}$ is found to be approximately 2.

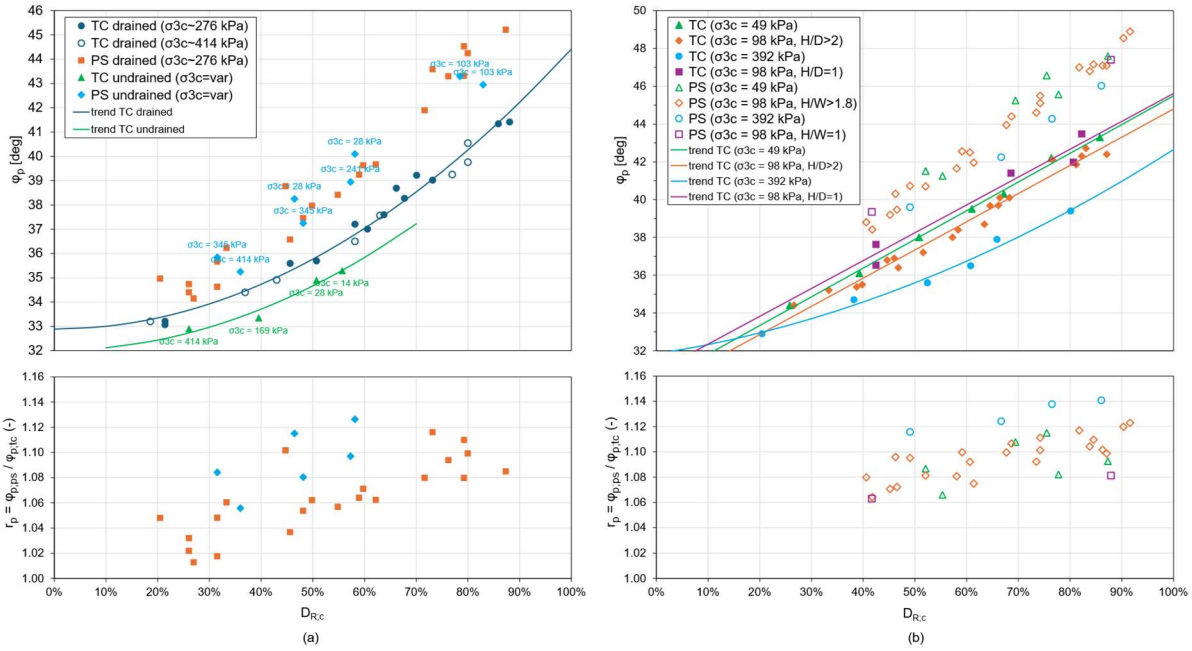


Fig 10: Peak friction angle and r_p as a function of relative density including regression from TC tests: (a) Brasted sand [20], (b) Toyoura_1 sand [32,57,58,104]

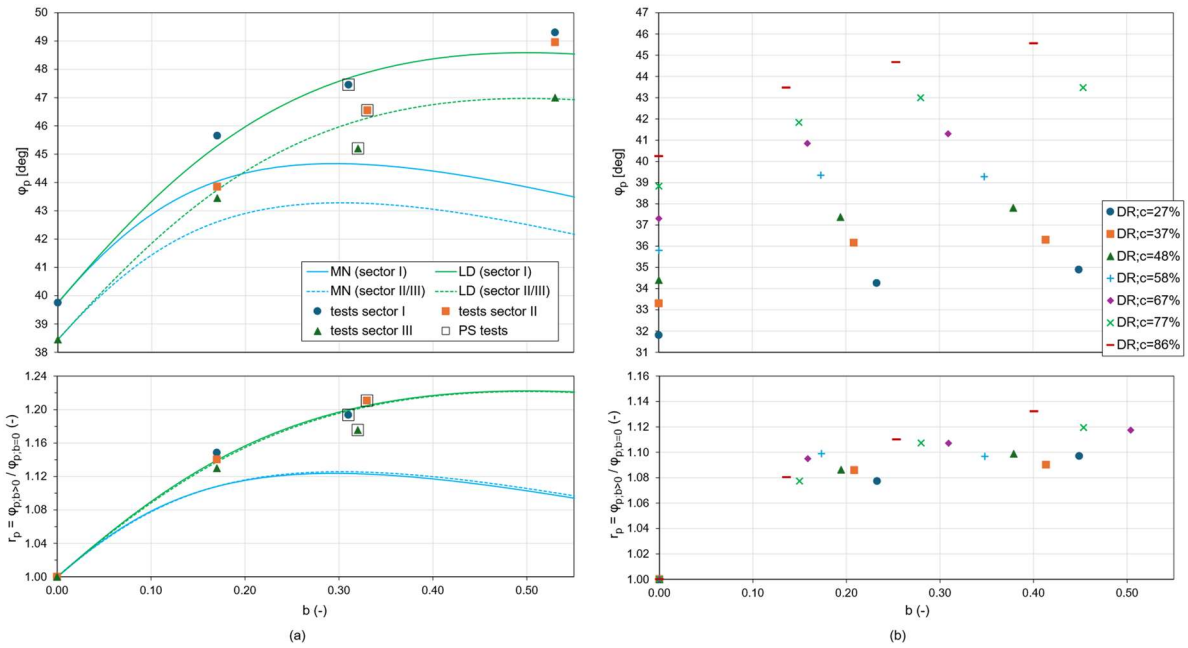


Fig 11: Peak friction angle and r_p as a function of b_p: (a) Cambria sand [70], (b) Loch Aline sand [100]

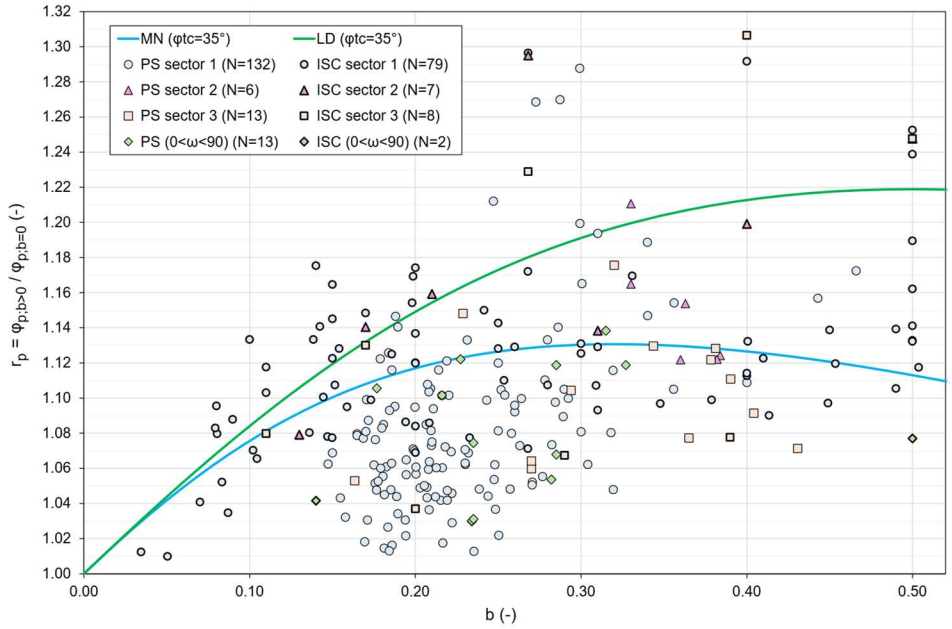


Fig 12: Data from all drained ISC and PS tests at which b was available from σ_2 measurements

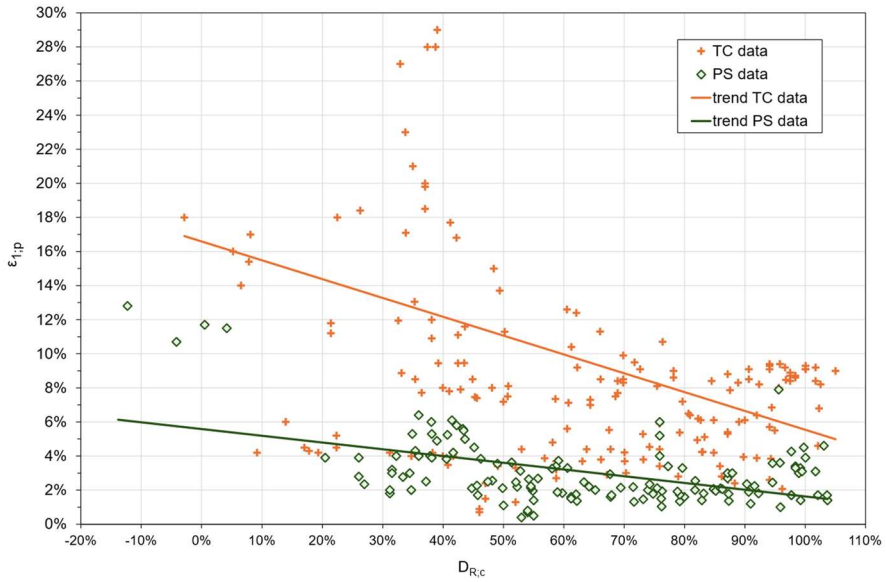


Fig. 13: Major principal strain (axial strain) at failure as a function of $D_{R;c}$ in sector 1 for drained TC/PS tests with σ_3<300 kPa

4.2 Evaluation of r_p from drained tests in sector 1

Drained tests in sector 1 form by far the largest part of the assembled database. This allows for performing a sensible statistical analysis on this data to investigate the influence of the factors discussed in section 2. It is noted that in the remainder of this section only ISC tests are included in the range of 0.14<b_p<0.47. These boundaries are selected by examining the minimum (0.147) and maximum (0.466) values of b_p found in all drained PS tests (N=163) in which σ_2 was measured, closely resembling the range indicated by [74].

As part of the exploratory data analysis, Fig. 14 presents the values of r_p are as a function of $D_{R;c}$. When all confining stresses are considered, a weak trend is found for $D_{R;c}$, as shown in Fig 14a. This has been exemplified by inclusion of the 90% confidence interval (CI) of the mean [18]. The trend becomes more pronounced, when a capping value of σ_3<300 kPa (Fig 14b). The most significant shift in trends from the cut-off is caused by omitting the data on Painted Rock dam material [4] and Crushed Napa basalt [3]. These materials have been tested at high relative densities (~70% and 100%) under (very) high confining stresses, resulting in relatively low r_p values.

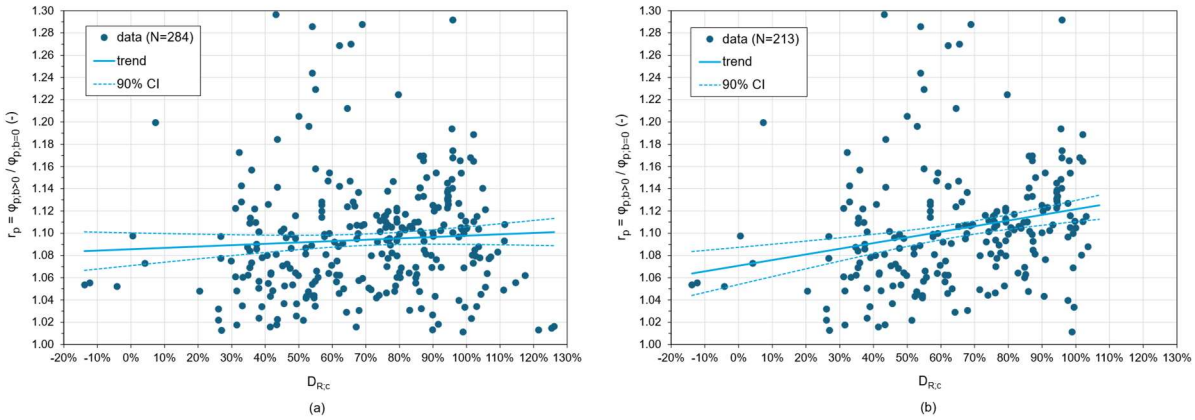


Fig. 14: Exploratory data analysis of r_p as a function of $D_{R;c}$: (a) for all values of σ_3, (b) tests with σ_3<300 kPa

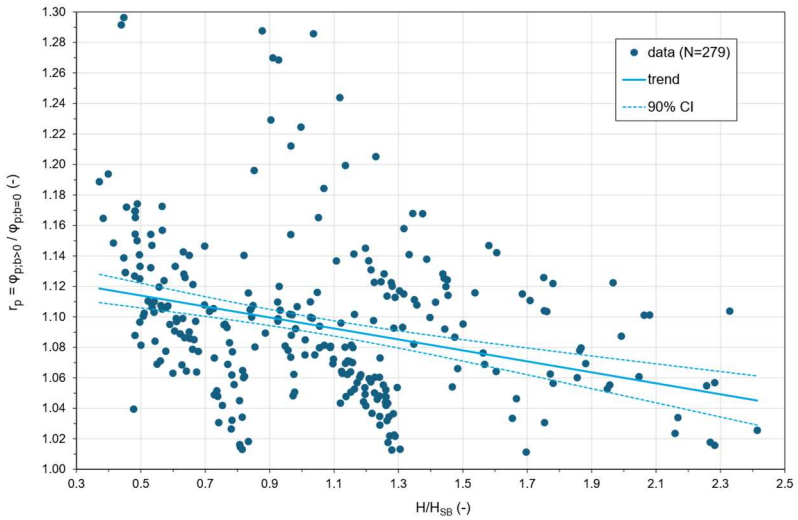
To isolate the effect of σ_3 on the results, the average values of r_p at different cut-off values are presented in Table 7. It can be seen that $\bar{r}_p$ decreases as the cut-off value of σ_3 increases for both the ISC and PS tests results. The average value of r_p from all ISC tests is remarkably close to 9/8 (=1.125).

Table 7: Effect of confining stress level on averaged r_p values

	$\sigma_3 \leq 50$ kPa		$\sigma_3 \leq 100$ kPa		$\sigma_3 \leq 300$ kPa		$\sigma_3 \leq 600$ kPa		all	
	N	$\bar{r}_p$	N	$\bar{r}_p$	N	$\bar{r}_p$	N	$\bar{r}_p$	N	$\bar{r}_p$
ISC	21	1.146	26	1.139	50	1.126	50	1.126	50	1.126
PS	19	1.123	80	1.104	165	1.096	196	1.093	236	1.086
both	40	1.135	106	1.112	215	1.103	246	1.100	286	1.093

516

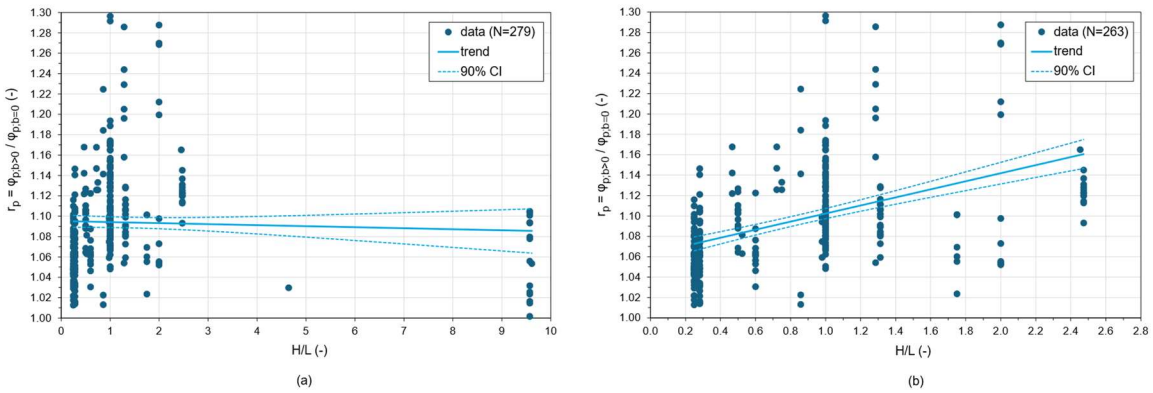
517 The trend of r_p with H/H_{SB} is presented in Fig. 15 including the 90% confidence interval of the mean. The overall
518 trend observed from the compiled database is significantly more pronounced than the distinction discussed
519 previously between groups 1 and 2 in Table 1.



520

521 Fig. 15: Exploratory data analysis: r_p as a function of H/H_{SB}

522 In addition to the H/H_{SB} ratio, the effect of the ratio H/L on r_p is investigated. Fig 16a shows no clear trend, when
523 all data is considered. It is clear however that the trend is strongly influenced by the data at H/L=9.57 (and one
524 data point at H/L=4.65). All these data points are obtained from Hostun sand [25,26,27]. These PS tests were
525 conducted using an unusually narrow apparatus. When the data of Hostun sand is omitted, a clear trend with H/L
526 is observed, as shown in Fig16b. Although it was not originally intended to account for the effects of boundary
527 conditions, type of lubrication and corrections, the trend in Fig16b seems to indicate that the length of specimen
528 plays a significant role in explaining the observed values of r_p. For this reason, the parameter H/L will be included
529 in the subsequent MLR analysis. The significance of the length and the deviation of Hostun sand from the observed
530 trend are discussed in section 5.2.



531

532 Fig. 16: Effect of H/L on r_p: (a) including data on Hostun sand, (b) excluding data on Hostun sand

533 An MLR analysis is performed on the drained dataset in sector 1 using the *clean* parameters $D_{R;c}$, H/H_{SB} and H/L.
534 The confining stress is made dimensionless using the equation commonly used to describe the stress-dependency

of stiffness of cohesionless soils [44], i.e. $(\sigma_3/p_a)^{0.5}$, in which p_a is the atmospheric pressure. The outcome and performance of the MLR analysis is presented in Table 8, including and excluding the data of Hostun sand. Given the low p-values, all predictors are significant. The standard error of the predicted value of r_p is given by σ_{r_p}. Prediction accuracy is highest for the MLR analysis excluding Hostun sand. In the remainder of the paper we use these results.

Table 8: Results of MLR analysis for estimated r_p from drained tests in sector 1

	excluding Hostun sand n=254, R^2=0.442, R^2_{adj}=0.433, σ_{r_p} = 0.0402			including Hostun sand n=270, R^2=0.339, R^2_{adj}=0.329, σ_{r_p} = 0.0436		
parameter	**coefficient**	**standard error**	**p-value**	**coefficient**	**standard error**	**p-value**
Intercept	1.125	$1.300 \cdot 10^{-2}$	$8.074 \cdot 10^{-188}$	1.156	$1.234 \cdot 10^{-2}$	$3.807 \cdot 10^{-205}$
$D_{R;c}$	$3.694 \cdot 10^{-2}$	$1.126 \cdot 10^{-2}$	$1.179 \cdot 10^{-3}$	$3.210 \cdot 10^{-2}$	$1.180 \cdot 10^{-2}$	$6.943 \cdot 10^{-3}$
$(\sigma_3/p_a)^{0.5}$	$-2.221 \cdot 10^{-2}$	$3.057 \cdot 10^{-3}$	$4.789 \cdot 10^{-12}$	$-2.806 \cdot 10^{-2}$	$2.895 \cdot 10^{-3}$	$3.275 \cdot 10^{-19}$
H/L	$3.099 \cdot 10^{-2}$	$4.913 \cdot 10^{-3}$	$1.286 \cdot 10^{-9}$	$3.002 \cdot 10^{-3}$	$1.531 \cdot 10^{-3}$	$5.104 \cdot 10^{-2}$
H/H_{SB}	$-4.452 \cdot 10^{-2}$	$7.065 \cdot 10^{-3}$	$1.335 \cdot 10^{-9}$	$-4.091 \cdot 10^{-2}$	$7.559 \cdot 10^{-3}$	$1.400 \cdot 10^{-7}$

To visualize the MLR prediction accuracy and how the results are smoothened, four subsets of the underlying data are made based on confining stress and sample geometry. The average values of the MLR input parameters for each subset are presented in Table 9. Fig 17 shows for each subset: (i) the measurement data, (ii) the predicted r_p for each data point based on the MLR, and (iii) the trends using the average values for each subset from Table 9 as input in the MLR. Comparison of subsets 2 and 4 to 1 and 3 shows that predicted values of r_p are (slightly) lower at higher values of σ_3. Comparison of subsets 3 and 4 to 1 and 2 reveals that the predicted values of r_p are considerably higher for cubical samples.

Table 9: Data subsets to visualize prediction accuracy of the MLR analysis

	stress range	H/W	H/L	N	$D_{R;c;avg}$	$\sigma_{3;avg}$	$(H/L)_{avg}$	$(H/W)_{avg}$	$(H/H_{SB})_{avg}$
subset	[kPa]	[-]	[-]	[-]	[%]	[kPa]	[-]	[-]	[-]
1	σ_3<100 kPa	>1.5	<0.75	17	63.8	88	0.60	3.37	1.712
2	100<σ_3<300 kPa	>1.5	<0.75	40	59.2	277	0.25	2.00	1.182
3	σ_3<100 kPa	<1.5	>0.75	14	70.7	54	1.00	1.00	0.485
4	100<σ_3<300 kPa	<1.5	>0.75	29	67.2	184	1.00	1.00	0.555

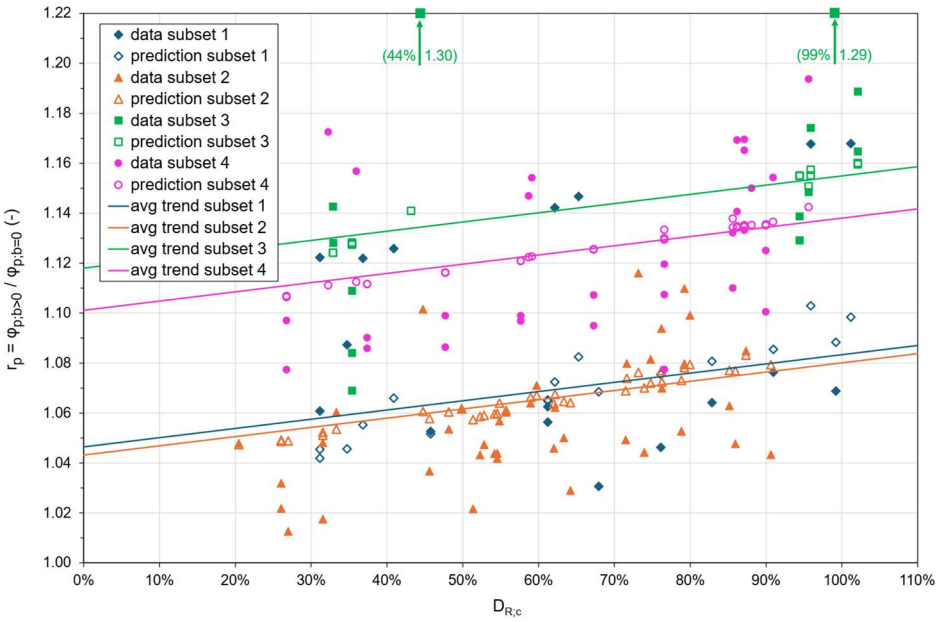


Fig. 17: Visualization of MLR performance (excluding Hostun sand) on subsets of the underlying data from Table 9

4.3 Results from other sectors in the octahedral plane

The quantity of experimental data from sectors 2 and 3 (and intermediate values of ω) is too limited to perform meaningful statistical analyses. Table 10 presents the mean of the tests in all sectors, capping the results for sector 1 at $\sigma_3 \leq 300$ kPa as the results for all other results are within this range. Again the b-values for ISC tests fall within the range $0.14 < b_p < 0.47$. On average no clear distinction is found between sector 1 and sector 3, but sector 2 appears to indicate higher values of r_p.

Table 10: Effect of confining stress level on averaged values of r_p

	sector 1		sector 2		sector 3		no sector	
	N	$\bar{r}_p$	N	$\bar{r}_p$	N	$\bar{r}_p$	N	$\bar{r}_p$
ISC	50	1.126	5	1.186	6	1.141	0	-
PS	165	1.098	6	1.150	20	1.083	13	1.076
both	215	1.104	11	1.166	26	1.096	13	1.076

In Fig 11a, typical results are shown for tests on Cambria sand in which no significant shear banding occurred (see Table 1). The difference in r_p between sector 2 and sector 3 is limited. Similar tests with cubical samples on Santa Monica Beach_2 sand [1] show more pronounced differences between sectors, but these results are not presented here. Instead, (some of) the results of tests performed on Toyoura_1 sand [32,57,58,104] are shown. Only tests at σ_3=98 kPa with H/D and H/W>1.8 are considered. The tests falling within sectors 1, 2 or 3 of the octahedral plane, as discussed in section 2.4, are presented in Fig 18. By further selecting ranges of $D_{R;c}$ these results can be compared to tests performed at intermediate values of ω (see Fig. 7). This comparison is made in Fig 19, indicating the effect of the rotation of the bedding plane on φ_p for both TC and PS tests. There is no need to plot the values of r_p to notice that the r_p values in sector 2 are significantly higher than in sector 3. In Fig 19a,c, at ξ=90° a dip is observed at ω=60°, indicating that the bedding plane is closely aligned with the shear band orientation β. These results are in agreement with those reported by [71] for Toyoura_3 sand. In Table 10, these results are included in the column *no sector* contributing to the lower value of $\bar{r}_p$ in that case.

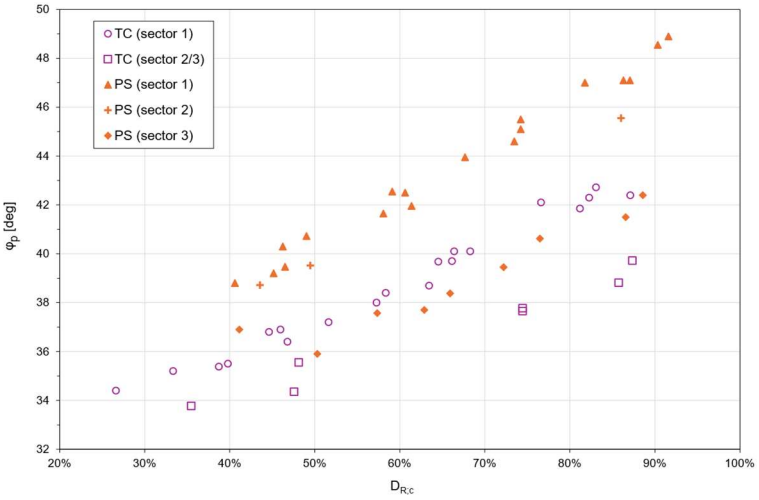


Fig. 18: Friction angle as a function of $D_{R;c}$ for a selection of data on Toyoura_1 sand (σ_3=98 kPa, H/D, H/W> 1.8)

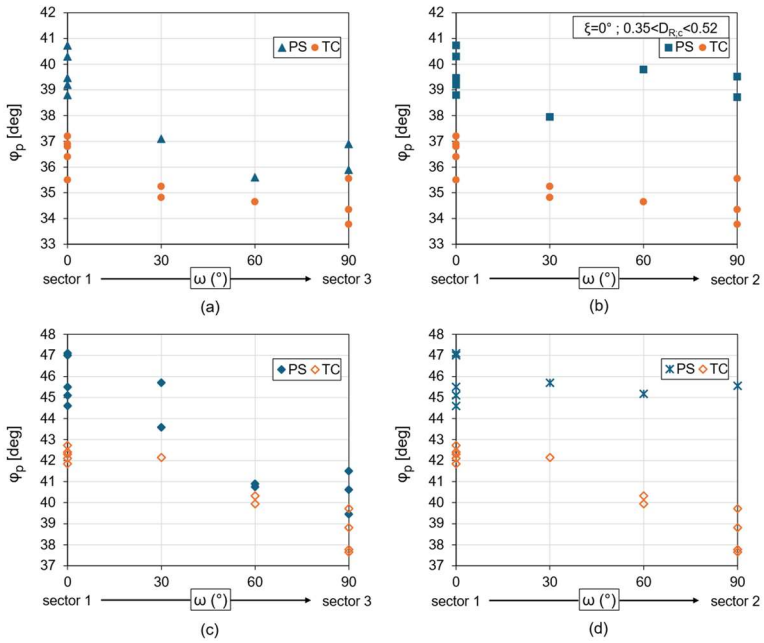


Fig. 19: Friction angle as a function of ω: (a) at ξ=90° for medium-low relative densities, (b) at ξ=0° for medium-low relative densities, (c) at ξ=90° for high relative densities, (d) at ξ=0° for high relative densities

4.4 Results from undrained tests

Similar to different sectors in the deviatoric plane, the available experimental data on undrained tests is insufficient to perform meaningful statistical analyses. In addition, the failure condition is not defined equally for undrained tests in all studies, see section 2.1. Therefore, only some typical results are presented. Undrained tests on Brasted sand [20] at the f2 condition are presented in Fig 10a. Values of $\varphi_{f2;tc}$ are integrally lower than $\varphi_{p;tc}$ and despite the confining stresses varying strongly, no clear effect of this is visible on $\varphi_{f2;tc}$. The undrained PS tests show very similar results to drained PS tests. At intermediate relative densities, two tests result in higher values of $\varphi_{f2;ps}$ at lower confining stresses. From these observations it follows that (slightly) higher values of r_p are found in the undrained tests, as visualized in Fig 10a. Comparative results from drained and undrained tests on Antioch sand [59] and Painted Rock dam material [4] are presented in Fig. 20 and Fig. 21 respectively. In both cases, the undrained strengths are determined at the f1 condition. For Painted Rock dam material, the values of φ_{f1} are lower than the corresponding values of φ_p from drained tests, and the effects of relative density and confining on φ_{f1} are in qualitative agreement for the drained and undrained tests. The values of φ_{f1} for Antioch sand show no clear dependency on both confining stress and relative density.

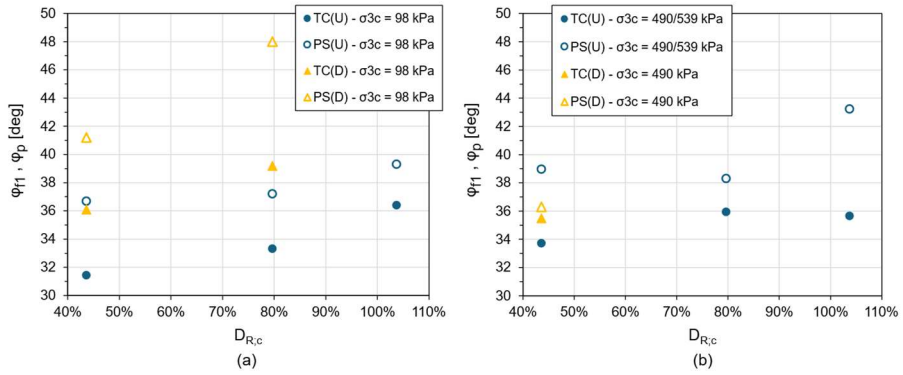


Fig. 20: Friction angle at $(\sigma_1-\sigma_3)_{max}$ as a function of $D_{R;c}$ for drained and undrained tests on Antioch sand [59]: (a) at σ_{3c} = 98 kPa, (b) at $\sigma_{3c} \approx$ 500 kPa

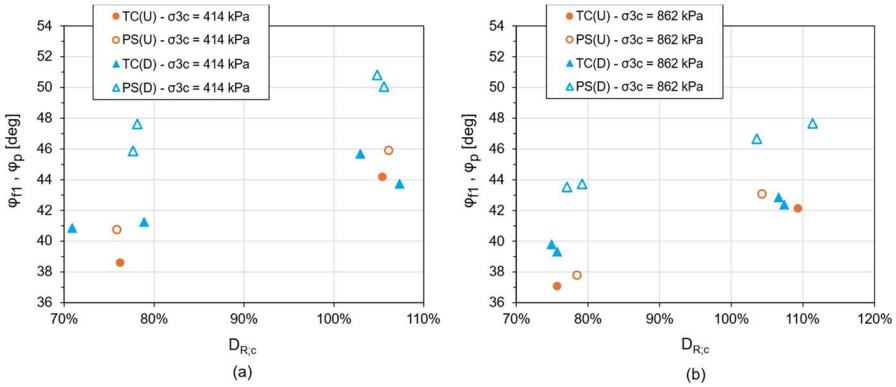


Fig. 21: Friction angle at $(\sigma_1-\sigma_3)_{max}$ as a function of $D_{R;c}$ for drained and undrained tests on Painted Rock dam material [4]: (a) at σ_{3c} = 414 kPa, (b) at σ_{3c} = 862 kPa

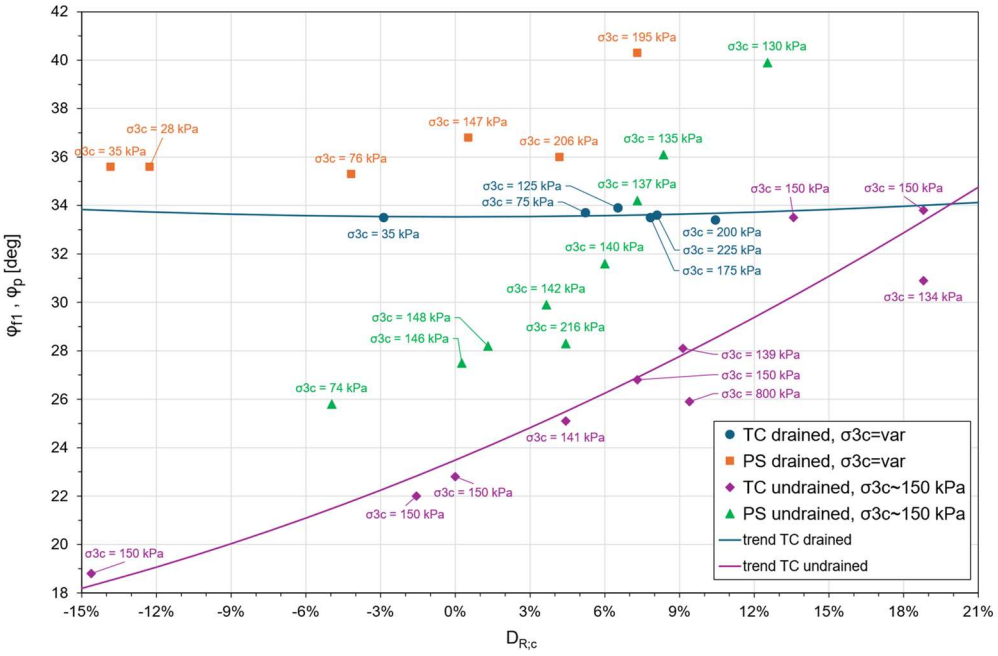
4.5 Results on critical state friction angle

As noted in section 2.1, it is assumed implicitly by [14] and explicitly by [91] that the critical state friction angle is independent of the test configuration. This is consistent with the post-peak strengths observed in strain-controlled tests on Brasted sand [20]. Whether the TC and PS peak strengths at $D_{R;c}\approx0\%$ would also coincide as suggested by [21] is uncertain, as the lowest value of $D_{R;c}$ achieved in the tests was approximately 20% (see Fig 10a).

Most tests in the assembled database were conducted to obtain peak strengths and were terminated shortly after the peak was reached, if stress-strain details were provided at all. To obtain φ_c from an individual test, it needs to be assured that the dilation rate approaches zero. This can be accomplished either by continuing a strain-controlled test to a sufficiently high strain level, or by testing very loose samples that show no dilation.

Stress paths of drained tests on Skedsmo sand [76] indicate that the effective stress ratio σ_1/σ_3 stabilizes at similar values in both TC and PS conditions. The results are presented up to an axial strain of 5%, which is sufficient to achieve a near-zero dilation rate in the PS tests, but not entirely in the TC tests. Stress paths of drained ISC tests on dense Santa Monica Beach_1 sand [113] also indicate similar ratios of σ_1/σ_3 at the b=0 and b>0 tests. Several stress-strain results of drained tests on Toyoura_1 sand [57] indicate a lower stress ratios σ_1/σ_3 from TC tests than from PS tests, even as the axial strains in the TC tests are insufficient to reach a zero dilation rate. Results from undrained tests on Masonry sand [31] at very low relative densities ($D_{R;c}$=0-10%), analyzed with condition f2, indicate an average ratio $\varphi_{f2;ps}/\varphi_{f2;tc}$ of 1.039.

Both drained and undrained tests have been performed on Changi sand at very low relative densities. The results are presented in Fig 22. From the drained tests [115] an average r_p value of 1.089 is found (1.066 if the outlier at $D_{R;c}$=7% is excluded). Although confining stresses differ significantly in the drained TC tests, this has no apparent effect on φ_p. The undrained test results presented in Fig. 22 are tabulated at failure condition f1 [116], and these result in an average ratio $\varphi_{f1;ps}/\varphi_{f1;tc}$=1.220 with a clear dependency on $D_{R;c}$. All undrained tests below $D_{R;c}\approx10\%$ show instability behavior by increasing excess pore pressures. The stress obliquities at the end of the undrained tests appear to match very well to those of the drained tests, both in TC and PS conditions. This indicates that the ratio $\varphi_{f2;ps}/\varphi_{f2;tc}$ is similar to r_p from the drained tests.



626

627 Fig. 22: Friction angle as a function of relative density for drained and undrained tests on Changi sand

5. DISCUSSION

5.1 Governing factors and data analysis

In this study, a legacy experimental database of ISC and PS tests on sands is compiled to asses the magnitude of the plain strain strength surplus, r_p, and the factors governing it. Based on the findings by [7], the factors that influence the strength in triaxial compression are a.o. relative density and confining stress. This study confirms their importance, showing that both parameters influence r_p as well. The influence of relative density is evident, e.g. Fig. 10, although an opposite dependency on σ_3 is found for Toyoura_1 sand, as seen in Fig 10b.

Although particle angularity and uniformity have been shown to have an effect on strength [17], they are not considered in this study. Mean grain size diameter is evaluated in the context of shear band formation, using the auxiliary parameter H/H_{SB}, which proves to be a significant predictor in the performed MLR analysis. Referring to Fig. 5, the height required for a shear band to freely develop, H_{SB}, is estimated as $W\tan\beta+15d_{50}/\cos\beta$, where the last term refers to the typical shear band thickness [110], and β is estimated based on the Arthur orientation using an estimation of ψ based on φ_p.

In addition, the parameter H/L proves to be significant, which was not expected a priori as it has been assumed that lubrication and friction corrections would be adequate to limit the influence of the sample length on the results. It is striking that the results from the tests on Hostun sand form an exception, although these tests have (by far) the largest H/L ratios. Presumably, given the sample dimensions, this has been a key point of attention in that research such that significant effort has been put in minimizing, measuring and correcting for the side platen friction. It is therefore emphasized that the reason for excluding this data from the MLR analysis is *not* the quality of the data. It can not be concluded that in other studies efforts to correct for side platen friction are lacking, but the trend remains striking.

All used predictors in the MLR analysis are significant, but the overall prediction capacity remains limited with a maximum R^2=0.442. Apart from the discussion of including / excluding Hostun sand, no outliers have been deleted, nor has the effect of deleting outliers been evaluated. Although more advanced data analysis techniques (e.g. random forest, gradient boosting) can significantly upgrade the prediction capacity, these come at the expense of explainability. For this reason, the results from these efforts have been omitted in this paper.

5.2 Plane strain surplus for cohesionless soil

As discussed in the introduction of this paper, the value of 9/8 is not a constant, even under the assumptions of associative soil behavior and the validity of the MN yield surface. That r_p is, on average, lower than 9/8 is clearly visualized in Fig 12. The value of 9/8 is, however, remarkably close to the mean result of tests on cubical ISC tests at relatively low confining stresses, see Table 7. The presented MLR results are valuable to quantify, in an approximate manner, the effect of relative density and confining stress on r_p. The parameters H/L and H/H_{SB} only have meaning in an experimental setting, but are of limited value, when performing a geotechnical assessment in practice. The MLR expression can be reduced by choosing appropriate values of H/L and H/H_{SB}. A conservative value of H/L would be 0.25. This is the value of the apparatus first used by Imperial College [20,112] and later (approximately) in several other studies [3,4,5,42,43]. By comparing the values of r_p at H/L=0.25 in Fig. 16a with the values of r_p from Hostun sand (at H/L=4.65 and H/L=9.57), at this low ratio of H/L, the effect of side platen friction on the results appears to be minimized. The value of H/H_{SB} should be chosen such that either uniform or localized strain behavior is expected, i.e. that shear bands are (or are not) allowed to develop continuously. For uniform strain conditions, it is proposed to use the 5th percentile value from the data used in the MLR analysis (excluding Hostun sand), which results in H/H_{SB}=0.48 and consequently C=1.111 in Eq. 5. For the condition of localized strain, the 95th percentile value is proposed, which gives H/H_{SB}=1.76 and consequently C=1.054. This means that a difference of Δr_p=0.057 exists between uniform and localized strain conditions at equal confining stress and relative density.

$$r_p = \frac{\varphi_{p;ps}}{\varphi_{p;tc}} \approx C + D_{R;c} \cdot 3.694 \cdot 10^{-2} - \sqrt{\sigma_3/p_a} \cdot 2.221 \cdot 10^{-2} \qquad \text{Eq. 5}$$

By inverting Eq. 5, the contours of equal r_p values are plotted in Fig. 23 for both proposed C values. In Fig. 24 some of the underlying data is plotted on top of these contours to get a further sense of the prediction accuracy.

The numbers in Fig. 24 represent calculated r_p values from the database. Those without connectors are centered at the $(\sigma_3;D_{R;c})$ coordinate corresponding to the ISC or PS test. For ISC tests in Fig24a, the values of b_p are provided. Based on the ratio H/H_{SB} the results of Monterey_0 sand are plotted in the uniform strain domain, even as these results were categorized to be in group 2 by [55], see Table 1.

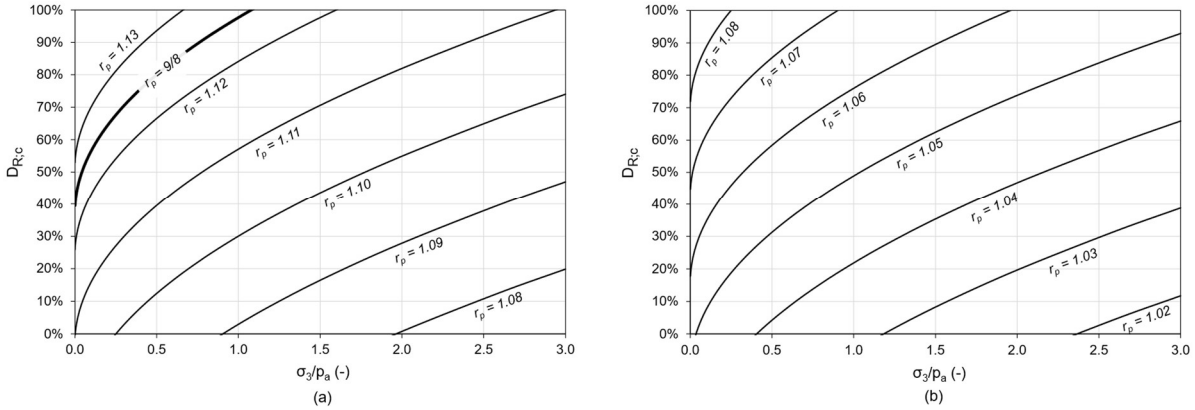


Fig. 23: Equal r_p curves as a function of relative density and confining stress: (a) for uniform strain conditions using C=1.111 in Eq. 5, (b) for localized strain conditions using C=1.054 in Eq. 5

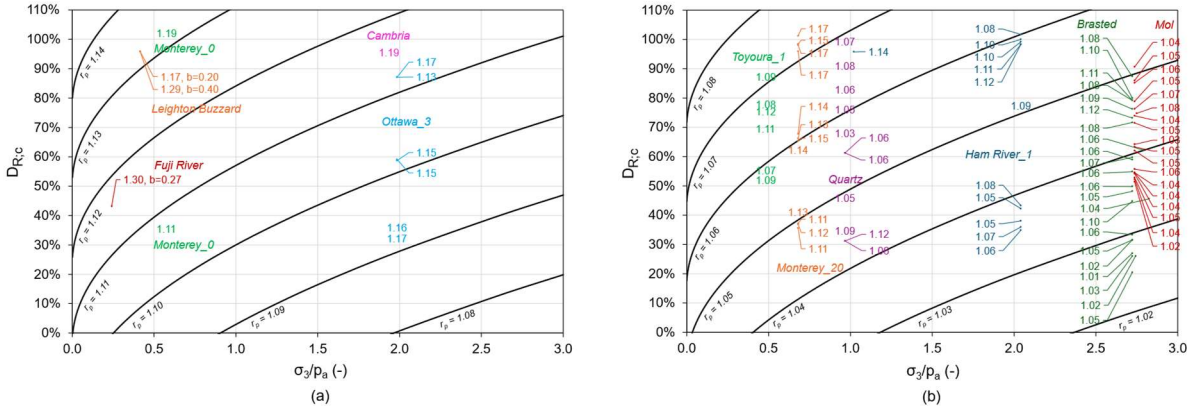


Fig. 24: Experimentally determined r_p values for a selected number of sands compared to the equal r_p curves: (a) for tests at which uniform strains are expected (b) for tests at which localized strains are expected

Without exception, all presented data in Fig24a exceeds the values of the corresponding curves. This is caused partly by the fact that all these tests are performed on cubical samples (H/L=1), while for the curves H/L=0.25 was used. However, this does not fully explain the deviations, i.e. there is still a significant exceedance if the curves are plotted using H/L=1. A better match between the data and curves is found for localized strain conditions in Fig24b, but again a significant portion of the experimental data exceeds the corresponding curves. The deviations for Toyoura_1 and Ham River_1 sands can be explained by their H/L ratios, which were 1.31 and 1.00, respectively. For Monterey_20 sand, the sample dimensions were varied such that H/H_{SB} ranges from 0.97 to 1.78 and H/L from 0.47 to 1. These variations cannot fully explain the observed deviations between the data and the curves. Finally, the r_p values of Mol sand appear to be consistently lower than those of Brasted sand, even tough the same apparatus with identical dimensions was used at Imperial College. In addition to possible apparatus adjustments or modifications, this could hint at a material dependency of r_p that is not accounted for in the current MLR analysis.

5.3 Applying plane strain strength in engineering practice

Peak strength

Given the experimental results assembled and presented in this paper, it is sensible to apply a higher peak strength than $\varphi_{p;tc}$ when analyzing geotechnical plane strain boundary value problems. For the case of a simple homogeneous slope, it has been illustrated in section 2.3 that adequately accounting for shear banding effects in

non-associative material requires a sufficiently fine mesh in FEM analyses and appropriate settings in a LEM environment. Considering the fictive case study in section 2.3, and assuming that the value of φ represents the peak friction angle from triaxial compression test(s), with $D_{R;c}$=0.56 (corresponding to $\varphi_{p;tc}$=35° [16]), σ_3≈40 kPa (based on the Plaxis 2D model), and H/L=0.25, the difference between H/H_{SB}=0.48 and H/H_{SB}=1.76 results in $\Delta\varphi_{p;ps}$≈2.0°. Based on LEM calculations, this corresponds to a change of factor of safety of ΔFoS≈0.09.

The difference between the results obtained from a very fine mesh in FEM and those obtained with a coarse mesh in FEM and the Mohr-Coulomb expression in LEM, depends strongly on the degree of non-associativity, see Table 2 and Table 3. The value of ψ=6.25° is chosen to represent the approximate but typical peak dilation angle corresponding to $\varphi_{p;tc}$=35°. At this dilatancy angle, ΔFoS between the coarsest and finest meshes in FEM is approximately 0.09, and ΔFoS between the Coulomb orientation in LEM and finest mesh in FEM is approximately 0.11.

In accordance with the introductory statement by [53], *the determination of a three-dimensional failure criterion for use in continuum-type constitutive models depends on reliable experimental data corresponding to uniform strain conditions in the specimen*, ideally all tests results are based on uniform strain conditions and shear banding should be appropriately accounted for in the model environment. In that line of thought, C=1.111 could be used in Eq. 5 and localization needs to be addressed separately in the model environment. However, a significant part of the PS tests are set up such that shear bands can freely develop, and from section 2.3, it can be seen that some effort is required from an engineering practice point of view to appropriately account for shear band development in model environments. This introduces unwanted mesh dependency in FEM and arbitrary results in LEM, if β is not appropriately calibrated.

An alternative approach would be to not address localization in the model environment, but instead use the plane strain strength surplus from tests in which localization occurred. This can be achieved by using C=1.054 in Eq. 5. Based on the presented results for the considered fictive case of a slope, this approach seems to provide reasonable results, as the ΔFoS from the varying C values correspond well to the difference between using a very fine mesh in FEM and using either a coarse mesh in FEM or the Mohr-Coulomb expression in LEM. The advantage of this approach is that a (somewhat lower) plane strain strength surplus is used, without the need to optimize the mesh in FEM and sticking to the familiar Mohr-Coulomb expression in LEM.

Although this alternative approach seems reasonable, we cannot substantiate this for the general case. The choices of the predictors and functional form of the MLR, and the choice of H/H_{SB} values representing uniform or localized strain behavior, are partly subjective. These have a direct effect on $\Delta\varphi_{p;ps}$. In addition, only one fictive case for a single type of boundary value problem has been evaluated. Recent FEM results indicate that the magnitude and distribution of bending moments in a retaining structure show similar mesh dependency effects for non-associative material behavior [28].

Conditioned on the values of H/L and H/H_{SB}, Eq. 5 gives a best estimate of r_p. To estimate a plane strain surplus for a specific project with an entirely different type of sand, it is useful to account for the uncertainty in this estimate. The characteristic value of the mean $r_{p;k}$ can be determined using Eq. 6. Herein r_p is the best estimate from Eq. 5, $t_{N-1}^{0.05}$ is the inverse of the student-t distribution with an exceedance probability of 5% based on N-1 samples, σ_{r_p} is the standard error of r_p found in Table 8 and N is the number of samples. Evidently, in principle any exceedance probability can be applied. In an engineering project context, one is more interested in the characteristic mean (of all samples) for a specific type of sand than the characteristic value of an individual sample. The 254 samples underlying the MLR analysis were obtained from tests on 25 different sands. Therefore, it seems sensible (and slightly conservative) to apply N=25. Referring to Fig. 23b, this will only result in values of $r_{p;k}$<1 for very loose sands at relative high confining stresses, which is in qualitative agreement with the experimental results.

$$r_{p;k} = r_p(D_{R;c}, \sigma_3) + \frac{t_{N-1}^{0.05}\sigma_{r_p}}{\sqrt{N}} = r_p(D_{R;c}, \sigma_3) - 0.0138 \geq 1 \qquad \text{Eq. 6}$$

Critical strength

Most of the experiments in the database and the analyses in this paper focus on the peak strength of sands. Presumably, the critical strength is more appropriate for assessing slope stability. Considering the results in section 4.5, it is not evident whether in general a strength surplus is found in critical state conditions. The most conservative option is therefore to assume no surplus. This approach is somewhat contradictory, given that r_p is higher than 1 at very low relative densities. Alternatively, Fig23b could be used at $D_{R;c}$=0%. This leads to values of $r_c=\varphi_{c;ps}/\varphi_{c;tc}$ that are approximately found for Changi and Masonry sand. However, these values of r_c and the dependency on σ_3 expressed through Eq. 5 are not thoroughly substantiated by data. It is in any case preferred over applying the LD or MN yield surfaces in a FEM environment, as these are guaranteed to overpredict the strength at critical state conditions, see Fig. 1 and section 2.1.

Inherent anisotropy

In engineering practice, constitutive models for sands generally assume isotropic material behavior. Despite the limited quantity of data outside sector 1 of the octahedral plane, it is studied in section 4.3 that inherent anisotropy of a layered soil has a significant impact on the absolute strengths found in experimental conditions. In terms of a plane strain surplus, based on the results in Table 10, the value of r_p in sector 3 seems comparable to sector 1. However, if shear bands can form perpendicular to the bedding plane, as shown in Fig. 19a,c, the results obtained from data in sector 1, may be too optimistic. The required effort to address this issue is significant: (a) more experimental data is required, (b) the effect of deposition techniques used in an experimental setting should be related to the effect of in-situ (site specific) soil deposition and (c) model environments should be able to account for the anisotropic material behavior of sands. In this context, the results obtained from the data on sector 1 are believed to be acceptable for engineering purposes when the behavior of sands is modelled isotropically.

6. CONCLUSIONS

This study has examined the factors that determine the peak strength measured in plane strain conditions and, consequently, the surplus compared to triaxial compression conditions, designated as the ratio r_p. Relative density and (effective) confining stress have a significant influence on both the peak friction angle measured in triaxial compression and on r_p. As such these factors have a reinforcing effect on the measured peak strength in plane strain, i.e. they affect $\varphi_{p;ps}$ more strongly than $\varphi_{p;tc}$. Effects of inherent anisotropy introduced by the direction, in which the sample was built, also play an important role. In this study, this is mainly accounted for by separating the data from different sectors in the deviatoric plane before investigating the effect of other variables.

Sample dimensions have a significant effect on the measured strength. The height of the sample H relative to the (estimated) height for a shear band to develop freely, H_{SB}, has a significant influence on r_p. As localization in shear bands can occur in the hardening regime of plane strain tests, these suppress the peak strengths reached in the tests when they can freely develop. The sample height relative to its length, H/L, was a priori not expected to have a significant influence, but the data indicate otherwise. Presumably, side platen interaction or friction has a more pronounced effect on the results the lower the height of the sample relative to its length (the distance between the zero strain boundaries in a PS test).

A database of both PS and ISC tests (falling in the range of intermediate principal stresses typically corresponding to plane strain) was assembled. For drained tests in sector 1, sufficient data have been assembled to perform a multi-linear regression analysis, which can be used to quantify the effect of the variables described above on the expected value of r_p. A relatively simple analysis and set of parameters were deliberately chosen to explain the governing parameters and their quantitative effect as clearly as possible. Overall, this study extracted trends from the combined legacy experimental data that could not be derived from the individual studies in isolation.

By proposing a sensible value of H/L and two distinct values of H/H_{SB}, two similar relations were obtained, where r_p is expressed as a function of confining stress and relative density. The distinct values and thereby the relations are used to distinguish between uniform and localized strain conditions, indicating whether shear bands can freely develop. Using a fictive case of a homogeneous slope from literature, FE and LE analyses were performed, in which the possibility of shear band formation was adequately and inadequately accounted for. It is found that the differences in terms of the calculated factor of safety FoS are comparable to the difference that follows from the derived relations from experimental data for uniform and localized strain conditions.

Based on these results, it is emphasized that adequately accounting for the plane strain strength puts restraints on the model environment in which it is applied. Specifically, localized strain behavior in non-associative materials should be properly represented. The findings suggest that the peak strength can be adjusted depending on the sophistication of the model environment. No restraints on the model environment such as currently implemented in the Dutch National Annex to Eurocode 7 is unwise. In that case one should be careful and it is recommended to use the derived relation for localized strain conditions, possibly reduced to account for the uncertainty in the estimate of r_p. A thorough parametric study for varying boundary value problems is recommended to assess what settings/conditions are required to properly account for shear bands in model environments, as to apply the correct plane strain surplus.

Regarding the plane strain strength surplus at critical state, one should be even more cautious as the experimental substantiation thereof is limited, both quantitatively and qualitatively. In this respect, the use of a MN or LD yield surface in FEM for boundary value problems involving large shear strains is not recommended.

Overall, the relevance of these findings is two-fold. If there is consensus on a conservative plane strain strength surplus for cohesionless soils that is not yet accounted for, this has a large potential in terms of material and assessment of existing infrastructure both for design as well as lifetime extension. If a plane strain strength surplus is applied according to a current code provision and is higher than what can be expected or substantiated, this may imply that geotechnical stability and/or structural safety is overestimated.

ACKNOWLEDGMENTS

The authors gratefully acknowledge the Port of Rotterdam for initiating, funding and enabling this research. In particular, we would like to thank Alfred Roubos for his continued trust, freedom and patience that were invaluable to the successful completion of this work.

DATA AVAILABILITY

The compiled database and generated data in this study are available from the corresponding author upon reasonable request.

DECLARATIONS

Conflict of interest

The authors declare that they have no known competing financial interests or personal relationships that could have appeared to influence the work reported in this article.

REFERENCES

1. Abelev AV, Lade PV (2003) Effects of Cross Anisotropy on Three-Dimensional Behavior of Sand. I: Stress-Strain Behavior and Shear Banding. J. Eng. Mech. 129(2):160-166. https://doi.org/10.1061/(ASCE)0733-9399(2003)129:2(160)
2. Abelev AV, Lade PV (2004) Characterization of Failure in Cross-Anisotropic Soils. J. Eng. Mech. 130(5):599-606. https://doi.org/10.1061/(ASCE)0733-9399(2004)130:5(599)
3. Al-Hussaini MM (1971) Drained plane strain and triaxial compression tests on crushed Napa basalt. USAE WES, Vicksburg, Mississippi, Technical Report S-71-2, Report 2. https://apps.dtic.mil/sti/citations/AD0756121
4. Al-Hussaini MM (1972) Plane strain and triaxial compression tests on Painted Rock dam material. USAE WES, Vicksburg, Mississippi, Technical Report S-71-2, Report 3. https://apps.dtic.mil/sti/citations/AD0756122
5. Al-Hussaini MM (1973) Influence of Relative Density on the Strength and Deformation of Sand under Plane Strain Conditions. Evaluation of Relative Density and Its Role in Geotechnical Projects Involving Cohesionless Soils, ASTM STP 523:332-347. https://doi.org/10.1520/STP523-EB
6. Alshibli KA, Batiste SN, Sture S (2002) Strain Localization in Sand: Plane Strain versus Triaxial Compression. J. Geotech. Geoenviron. Eng. 129(6):483-494. https://doi.org/10.1061/(ASCE)1090-0241(2003)129:6(483)
7. Anderson KH, Schjetne K (2013) Database of Friction Angles of Sand and Consolidation Characteristics of Sand, Silt and Clay. J. Geotech. Geoenviron. Eng. 139(7):1140-1155. https://doi.org/10.1061/(ASCE)GT.1943-5606.0000839
8. Arthur JRF, Menzies BK (1972) Inherent anisotropy in a sand. Géotechnique 22(1):115-128. https://doi.org/10.1680/geot.1972.22.1.115
9. Arthur JRF, Dunstan T, Al-Ani QAJL, Assadi A (1977) Plastic deformation and failure in granular media. Géotechnique 27(1):53-74. https://doi.org/10.1680/geot.1977.27.1.53
10. Arthur JRF, Dunstan T (1982) Rupture layers in granular media. IUTAM Conference on Deformation and Failure of Granular Materials:453-456 (eds. Vermeer PA, Luger HJ). AA Balkema, Rotterdam.
11. ASTM (2000) ASTM D4253-00: Standard Test Methods for Maximum Index Density and Unit Weight of Soils Using a Vibratory Table. https://doi.org/10.1520/D4253-00
12. Bentley (2024) Plaxis 2D 2024.2 Materials Models Manual 2D
13. Bishop AW (1966) The Strength of Soils as Engineering Materials. Géotechnique 16(2):91-130. https://doi.org/10.1680/geot.1966.16.2.91
14. Bolton MD (1986) The Strength and Dilatancy of Sands. Géotechnique 36(1):65-78. https://doi.org/10.1680/geot.1986.36.1.65
15. Boyle SR (1995) Deformation Prediction of Geosynthetic Reinforced Soil Retaining Walls. PhD thesis. University of Washington. http://hdl.handle.net/1773/10201
16. Brinkgreve RBJ, Engin E, Engin HK (2010) Validation of empirical formulas to derive model parameters for sands. Numerical Methods in Geotechnical Engineering:137-142 (eds. Benz T, Nordal S). CRC Press, London. https://doi.org/10.1201/b10551
17. BSI (2015) BS8002:2015 Code of practice for earth retaining structures
18. Calle E, Van Duinen, A (2016) Bepaling karakteristieke waarden schuifsterkte parameters (in Dutch). Memo 1220132-003-GEO0002. Deltares, Delft.
19. CIRIA (2003) CIRIA C580: Embedded retaining walls - guidance for economic design.
20. Cornforth D (1961) Plane Strain Failure Characteristics of a Saturated Sand. PhD thesis. Imperial College of Science and Technology. http://hdl.handle.net/10044/1/13682
21. Cornforth D (1964) Some Experiments on the Influence of Strain Conditions on the Strength of Sand. Géotechnique 14(2):143-167. https://doi.org/10.1680/geot.1964.14.2.143
22. Coulomb (1776). Essai sur une application des règles de maximis et minimis à quelques problèmes de statique, relatifs à l'architecture. Mémoires de Mathématique et de Physique présentés à l'Académie Royale des Sciences et lus dans ses Assemblées 7:343-382.
23. Davis EH (1968) Theories of Plasticity and the Failure of Soil Masses. Soil Mechanics - Selected Topics:341-380 (ed. Lee IK). Butterworths, London.

24. Deltares (2024) User Manual D-Stability, Version 2024.01
25. Desrues J, Hammed W (1989) Shear banding dependency on mean stress level in sand. 2nd International workshop on Numerical Methods for Localization and Bifurcation of Granular Bodies:57-67
26. Desrues J, Viggiani G (2004) Strain localization in sand: an overview of the experimental results obtained in Grenoble using stereophotogrammetry. Int. J. Numer. Anal. Meth. Geomech. 28:279-321. https://doi.org/10.1002/nag.338
27. Desrues (2023) Strain Localisation In Hostun Sand ALERT Modelling Benchmark https://doi.org/10.13140/RG.2.2.31848.24321
28. Dhauri SR (2025) Evaluating dilation and mesh dependency in geotechnical FEM simulations using non-associated plasticity. MSc Thesis. Delft University of Technology. https://resolver.tudelft.nl/uuid:7b31ebe9-9358-4b51-b9a6-a3a7bdee2ec8
29. EAU (2000) Recommendations of the Committee for Waterfront Structures Harbours and Waterways EAU 1996 - 7th English Edition. Ernst & Sohn, Berlin. ISBN 3-433-01790-5
30. Finno RJ, Harris WW, Mooney MA, Viggiani G (1997) Shear bands in plane strain compression of loose sand. Géotechnique 47(1):149-165. https://doi.org/10.1680/geot.1997.47.1.149
31. Finno RJ, Harris, WW, Mooney MA, Viggiani G (1996) Strain Localization and Undrained Steady State of Sand. Journal of Geotechnical Engineering 122(6):462-473. https://doi.org/10.1061/(ASCE)0733-9410(1996)122:6(462)
32. Fukushima S, Tatsuoka F (1984) Strength and Deformation Characteristics of Saturated Sand at Extremely Low Pressures. Soils and Foundations 24(4):30-48. https://doi.org/10.3208/sandf1972.24.4_30
33. Galavi V (2021) DeltaSand: A state dependent double hardening elasto-plastic model for sand: Formulation and validation. Computers and Geotechnics 129:1-12. https://doi.org/10.1016/j.compgeo.2020.103844
34. Georgiadis K, Potts D, Zdravkovic L (2004) Modelling the shear strength of soils in the general stress space. Computers and Geotechnics 31(5):357-364. https://doi.org/10.1016/j.compgeo.2004.05.002
35. Green GE, Bishop AW (1969) A note on the drained strength of sand under generalized strain conditions. Géotechnique 19(1):144-149. https://doi.org/10.1680/geot.1969.19.1.144
36. Green GE, Reades DW (1975) Boundary conditions, anisotropy and sample shape effects on the stress-strain behaviour of sand in triaxial compression and plane strain. Géotechnique 25(2):333-356. https://doi.org/10.1680/geot.1975.25.2.333
37. Griffiths D (1990) Failure Criteria Interpretation Based on Mohr-Coulomb Criterion. Journal of Geotechnical Engineering 116(6):986-999. https://doi.org/10.1061/(ASCE)0733-9410(1990)116:6(986)
38. Griffiths D, Huang J (2009) Observations on the extended Matsuoka-Nakai failure criterion. Int. J. Numer. Anal. Meth. Geomech. 33:1889-1905. https://doi.org/10.1002/nag.810
39. Hanna A (2001) Determination of plane-strain shear strength of sand from the results of triaxial tests. Canadian Geotechnical Journal 38(6):1231-1240. https://doi.org/10.1139/t01-064
40. Holtz RD, Lee WF (2002) Internal Stability Analyses of Geosynthetic Reinforced Retaining Walls. Report WA-RD 532.1, University of Washington, Seattle. https://rosap.ntl.bts.gov/view/dot/42023
41. Houlsby GT (1991) How the Dilatancy of Soils Affects their Behaviour. Report Number OUEL 1888/91, University of Oxford, Oxford.
42. Ichihara M, Matsuzawa H (1970) Experiments on Shearing Characteristics of Dry Sand Under Plane Strain Condition and Axial Symmetric Strain Condition (in Japanese). Proc. JSCE 173:47-59. https://doi.org/10.2208/jscej1969.1970.47
43. Ichihara M, Matsuzawa H (1973) Application of Plane Strain Test to Earth Pressure. 8th ICSMFE:185-190, Moscow https://www.issmge.org/publications/publication/application-of-plane-strain-test-to-earth-pressure
44. Janbu N (1963) Soil Compressibility as Determined by Oedometer and Triaxial Tests. Proc 3rd European Conference on Soil Mechanics and Foundation Engineering 1:19-25, Wiesbaden.
45. Jefferies M, Been K (2006) Soil Liquefaction - A critical state approach. Taylor & Francis, London and New York

46. Khayatt AJ (1967) Some Incremental Stress-Strain Relations for Sand. PhD thesis. The Victorica University of Manchester. https://www.librarysearch.manchester.ac.uk/permalink/44MAN_INST/1r887gn/alma992991354296601631
47. Ko H (1966) Static Stress-Deformation Characteristics of Sand. PhD thesis. California Institute of Technology. https://doi.org/10.7907/WWZB-SM07
48. Kolbuszewski JJ (1948) An experimental study of the maximum and minimum porosities of sand. Proc 2nd International Conference on Soil Mechanics and Foundation Engineering:158-165, Rotterdam. https://www.issmge.org/publications/publication/an-experimental-study-of-maximum-and-minimum-porosities-of-sands
49. Kulhawy F, Mayne P (1990) Manual on Estimating Soil Properties for Foundation Design. Report EL-6800. Electric Power Research Institute, Palo Alto, California.
50. Lade PV, Duncan JM (1973) Cubical Triaxial Tests on Cohesionless Soil. Journal of the Soil Mechanics and Foundations Division 99(10):793-812. https://doi.org/10.1061/JSFEAQ.0001934
51. Lade PV, Duncan JM (1975) Elastoplastic Stress-Strain Theory for Cohesionless Soil. Journal of the Geotechnical Engineering Division 101(10):1037-1053. https://doi.org/10.1061/AJGEB6.0000204
52. Lade PV (1977) Elasto-plastic stress-strain theory for cohesionless soil with curved yield surfaces. Int. J. Solids Structures 13(11):1019-1035. https://doi.org/10.1016/0020-7683(77)90073-7
53. Lade PV, Yamamuro JA, Skyers BD (1996) Effects of Shear Band Formation in Triaxial Extension Tests. Geotech. Test. J. 19(4):398-410. https://doi.org/10.1520/GTJ10717J
54. Lade PV, Wang Q (2001) Analysis of Shear Banding in True Triaxial Tests on Sand. J. Eng. Mech. 127(8):762-768. https://doi.org/10.1061/(ASCE)0733-9399(2001)127:8(762)
55. Lade PV (2006) Assessment of test data for selection of 3-D failure criterion for sand. Int. J. Numer. Anal. Meth. Geomech. 30:307-333. https://doi.org/10.1002/nag.471
56. Lade PV (2007) Modeling failure in cross-anisotropic frictional materials. International Journal of Solids and Structures 44(16):5146-5162. https://doi.org/10.1016/j.ijsolstr.2006.12.027
57. Lam W-K, Tatsuoka F (1988) Effects of Initial Anisotropic Fabric and σ2 on Strength and Deformation Characteristics of Sand. Soils and Foundations 28(1):89-106. https://doi.org/10.3208/sandf1972.28.89
58. Lam W-K, Tatsuoka F (1988) Triaxial Compressive and Extension Strength of Sand Affected by Strength Anistropy and Sample Slenderness. Advanced Triaxial Testing of Soil and Rock, ASTM STP 977:655-666. https://doi.org/10.1520/STP977-EB
59. Lee KL (1970) Comparison of Plane Strain and Triaxial tests on sand. Journal of the Soil Mechanics and Foundations Division 96(3):901-923. https://doi.org/10.1061/JSFEAQ.0001425
60. Leussink H (1965) Soil Properties - Shear Strength and Consolidation. Record of Technical Sessions, Session 2 - Division 2. 6th ICSMFE:302-306, Montréal. https://www.issmge.org/publications/publication/soil-properties-shear-strength-and-consolidation-5538
61. Leussink H, Wittke W, Wesseloh K (1966) Unterschiede im Scherverhalten rolliger Erdstoffe und Kugelschüttungen im Dreiaxial- und Biaxialversuch (in German). Veröffentlichungen des Institutes für Bodenmechanik und Felsmechanik der Technischen Hochschule Fridericiana in Karlsruhe - Heft 21. Karlsruhe.
62. Marachi ND, Duncan JM, Chan CK, Seed HB (1981) Plane-Strain testing of Sand. Laboratory Shear Strength of Soil, ASTM STP740:294-302. https://doi.org/10.1520/STP28758S
63. Matsuoka, H, Nakai, T (1974). Stress-Deformation and Strength Characteristic of Soil Under Three Different Principal Stresses. Proc. JSCE 232:59-70. https://doi.org/10.2208/jscej1969.1974.232_59
64. Merkle DH (1971) The effective stress Mechanics of Undrained Shear Strength. Technical Report AFWL-TR-71-85. https://apps.dtic.mil/sti/html/tr/AD0887071/index.html
65. Molenkamp F (1985) Comparison of friction material models with respect to shear band formation. Géotechnique 35(2):127-143. https://doi.org/10.1680/geot.1985.35.2.127
66. Mooney MA, Finno RJ, Viggiani MG (1998) A Unique Critical State for Sand? Journal of Geotechnical and Geoenvironmental Engineering 124(11):1100-1108. https://doi.org/10.1061/(ASCE)1090-0241(1998)124:11(1100)

67. Mühlhaus H-B, Vardoulakis I (1987) The thickness of shear bands in granular materials. Géotechnique 37(3):271-283. https://doi.org/10.1680/geot.1987.37.3.271
68. Nagaraj TS, Somashekar, BV (1979) Stress Deformation and Strength of Soils in Plane Strain. Proc of the 6th Asian Regional Conference on Soil Mechanics and Foundation Engineering 1:43-46. https://seags.ait.asia/publications/6th-ARC-1979-Singapore-v1.pdf
69. NEN (2017) NEN9997-1+C2:2017 nl - Geotechnisch ontwerp van constructies - Deel 1: Algemene regels (in Dutch).
70. Ochiai H, Lade PV (1983) Three-Dimensional Behavior of Sand with Anisotropic Fabric. Journal of Geotechnical Engineering 109(10):1313-1328. https://doi.org/10.1061/(ASCE)0733-9410(1983)109:10(1313)
71. Oda M, Koishikawa I, Higuchi T (1978) Experimental Study of Anisotropic Shear Strength of Sand by Plane Strain Test. Soils and Foundations 18(1):25-38. https://doi.org/10.3208/sandf1972.18.25
72. Peters JF, Lade PV, Bro A (1988) Shear Band Formation in Triaxial and Plane Strain Tests. Advanced Triaxial Testing of Soil and Rock, ASTM STP 977:604-627. https://doi.org/10.1520/STP977-EB
73. Potts D, Gens A (1984) The Effect of the Plastic Potential in Boundary Value Problems Involving Plane Strain Deformation. International Journal for Numerical and Analytical Methods in Geomechanics 8:259-286. https://doi.org/10.1002/nag.1610080305
74. Potts DM, Zdravković L (1999) Finite element analysis in geotechnical engineering - Theory. Thomas Telfort, London. https://doi.org/10.1680/feaiget.27534
75. Procter DC, Barden L (1969) A Note on the Drained Strength of Sand Under Generalized Strain Conditions (correspondence). Géotechnique 19(3):424-462. https://doi.org/10.1680/geot.1969.19.3.424
76. Quinteros VS, Fannin, RJ, Dyvik, R (2025) Peak Friction Angle of Sand at a Wide Range of Effective Stresses from Drained Direct Shear, Triaxial and Plane-Strain Tests for the Design of Retaining Structures. Geotech. Test. J. https://doi.org/10.1520/GTJ20240067
77. Ramamurthy T, Rawat PC (1973). Shear Strength of Sand Under General Stress System. 8th ICSMFE:339-342, Moscow. https://www.issmge.org/publications/publication/shear-strength-of-sand-under-general-stress-system
78. Ramamurthy T, Rawat PC, Tokhi VK (1981) Plane Strain Behaviour of Granular Medium. Indian Geotechnical Journal 11(4):301-326. https://igshq.in/igjbackvolumes/journals/Volume11/IGJ_11_04_301-326.pdf
79. Rawat PC, Ramamurthy T (1978) Shear Behaviour of Sand Under Generalized Conditions of Stress and Strain. Indian Geotechnical Journal 8(4):235-269. https://igshq.in/igjbackvolumes/journals/Volume08/IGJ_08_04_235-269.pdf
80. Reades DW, Green GE (1976) Independent stress control and triaxial extension tests on sand. Géotechnique 26(4):551-576. https://doi.org/10.1680/geot.1976.26.4.551
81. Reades DW (1972) Stress-strain characteristics of a sand under three-dimensional loading. PhD thesis. Imperial College of Science and Technology. http://hdl.handle.net/10044/1/20236
82. Roscoe KH (1970) The Influence of Strains in Soil Mechanics. Géotechnique 20(2):129-170. https://doi.org/10.1680/geot.1970.20.2.129
83. Rowe PW (1962) The Stress-Dilatancy Relation for Static Equilibrium of an Assembly of Particles in Contact. Proc. R. Soc. Lond. A 269:500-527. https://doi.org/10.1098/rspa.1962.0193
84. Rowe PW, Peaker K (1965) Passive Earth Pressure Measurements. Géotechnique 15(1):57-78. https://doi.org/10.1680/geot.1965.15.1.57
85. Rowe PW (1969) The Relation between the Shear Strength of Sands in Triaxial Compression, Plane Strain and Direct Shear. Géotechnique 19(1):75-86. https://doi.org/10.1680/geot.1969.19.1.75
86. Rudnicki JW, Rice JR (1975) Conditions for the Localization of Deformation in Pressure-Sensitive Dilatant Materials. J. Mech. Phys. Solids 23(6):371-394. https://doi.org/10.1016/0022-5096(75)90001-0
87. Runesson K, Ottosen NS, Perić D (1991) Discontinuous Bifurcations of Elastic-Plastic Solutions at Plane Stress and Plane Strain. International Journal of Plasticity 7(1-2):99-121. https://doi.org/10.1016/0749-6419(91)90007-L
88. Saada AS, Townsend FC (1981) State of the Art: Laboratory Strength Testing of Soils. Laboratory Shear Strength of Soil, ASTM STP740:294-302. https://doi.org/10.1520/STP28758S

89. Satake M (1982) On Equivalent Mohr Circle in Granular Materials. UNICIV Report R-205. University of New South Wales
90. Sayao ASFJ (1989) Behaviour of Sand under General Stress Paths in the Hollow Cylinder Torsional Device. PhD thesis. The University of British Columbia. https://doi.org/10.14288/1.0062539
91. Schanz T, Vermeer P. (1996) Angles of friction and dilatancy of sand. Géotechnique 46(1):145-151. https://doi.org/10.1680/geot.1996.46.1.145
92. Schweiger H, Tschuchnigg F (2022) Strength reduction technique with finite element method for slopes without stabilisation measures. Ground Engineering 5:27-34.
93. Shapiro S, Yamamuro JA (2003) Effects of Silt on Three-Dimensional Stress-Strain Behavior of Loose Sand. Journal of Geotechnical and Geoenvironmental Engineering 129(1):1-11. https://doi.org/10.1061/(ASCE)1090-0241(2003)129:1(1)
94. Social- og Boligstyrelsen (2021) DS/EN 1997-1 DK NA:2021 National Annex to Eurocode 7: Geotechnical Design - Part 1: General Rules
95. Sławińska (2018) The Mohr-Coulomb Friction Angle of Granular Soils Under Different Stress Conditions. Acta Sci. Pol. Architectura 17(4):51-60. https://doi.org/10.22630/ASPA.2018.17.4.40
96. Sławińska-Budzich J (2021) Characteristic parameter of soil failure criteria for plane strain conditions - experimental and semi-theoretical study. Studia Geotechnica et Mechanica 43(3):237-254. https://doi.org/10.2478/sgem-2021-0015
97. Sloan S (2013) Geotechnical stability analysis. Géotechnique 63(7):531-571. https://doi.org/10.1680/geot.12.RL.001
98. Sterpi D (2000) Influence of the kinematic testing conditions on the mechanical response of a sand. Computers and Geotechnics 26:23-41. https://doi.org/10.1016/S0266-352X(99)00033-6
99. Stroud MA (1989) The Standard Penetration Test - its applications and interpretation. Penetration Testing in the UK:29-49. Thomas Telfort, London
100. Sutherland H, Mesdary M (1969). The Influence of the Intermediate Principal Stress on the Strength of Sand. 7th ICSMFE:391-399, Mexico City. https://www.issmge.org/publications/publication/the-influence-of-the-intermediate-principal-stress-on-the-strength-of-sand
101. Świdziński W, Mierczyński J (2005) Instability Line as a Basic Characteristic of Non-Cohesive Soils. Archives of Hydro-Engineering and Environmental Mechanics 52(1):59-85. https://bibliotekanauki.pl/articles/241208.pdf
102. Symes MJPR (1983) Rotation of principal stresses in sand. PhD thesis. Imperial College of Science and Technology. http://hdl.handle.net/10044/1/7490
103. Symes MJPR, Gens A, Hight DW (1984) Undrained anisotropy and principal stress rotation in saturated sand. Géotechnique 34(1):11-27. https://doi.org/10.1680/geot.1984.34.1.11
104. Tatsuoka F, Sakamoto M, Kawamura T, Fukushima S (1986) Strength and Deformation Characteristics of Sand in Plane Strain Compression at Extremely Low Pressures. Soils and Foundations 26(1):65-84. https://doi.org/10.3208/sandf1972.26.65
105. Teunissen H (2016) Wrijving in sterkteberekeningen (in Dutch). Geotechniek 20(3):8-13.
106. Teunissen JAM (2022) The influence of the intermediate stress on the plane strain strength. Computers and Geotechnics 152. https://doi.org/10.1016/j.compgeo.2022.104983
107. Tsegaye AB, Benz T, Nordal S (2013) On the geometry of plastic potential surfaces and isochoric stress paths. 18th ICSMGE:667-671, Paris. https://www.issmge.org/publications/publication/on-the-geometry-of-plastic-potential-surfaces-and-isochoric-stress-paths
108. Vardoulakis I (1980) Shear Band Inclination and Shear Modulus of Sand in Biaxial Tests. Int. J. Num. Anal. Meth. Geomech. 4(2):103-119. https://doi.org/10.1002/nag.1610040202
109. Vermeer PA, de Borst R (1984) Non-Associated Plasticity for Soil, Concrete and Rock. HERON 29(3). https://heronjournal.nl/29-3/1.pdf
110. Vermeer PA (1990) The orientation of shear bands in biaxial tests. Géotechnique 40(2): 223-236. https://doi.org/10.1680/geot.1990.40.2.223
111. Viggiani G, Küntz M, Desrues J (2001) An experimental investigation of the relationships between grain size distribution and shear banding in sand. Continuous and Discontinuous Modelling of

Cohesive-Frictional Materials (Lecture Notes in Physics 568):111-127 (eds. Vermeer PA, Herrman HJ, Luding S, Ehlers W, Diebels S, Ramm, E). https://doi.org/10.1007/3-540-44424-6_8

112. Wade NH (1963) Plane strain failure characteristics of a saturated clay. PhD thesis. Imperial College of Science and Technology. http://hdl.handle.net/10044/1/17074

113. Wang Q, Lade PV (2001) Shear Banding in True Triaxial Tests and Its Effect on Failure in Sand. J. Eng. Mech. 127(8):754-76. https://doi.org/10.1061/(ASCE)0733-9399(2001)127:8(754)

114. Wanatowski D, Chu J (2007) Static liquefaction of sand in plane strain. Canadian Geotechnical Journal 44:299-313.

115. Wanatowski D, Chu J (2007) Drained behaviour of Changi sand in triaxial and plane-strain compression. Geomechanics and Geoengineering: An International Journal 2(1):29-39. https://doi.org/10.1080/17486020601173193

116. Wanatowski D, Chu J (2008) Undrained behaviour of Changi sand in triaxial and plane-strain compression. Geomechanics and Geoengineering: An International Journal 3(2):85-96. https://doi.org/10.1080/17486020701742608

117. Wightman A (1967) The Stress-Dilatancy of Sands During Plane Strain Compression. MSc Thesis. The Victorica University of Manchester.

118. Wroth C (1984). The interpretation of in situ soil tests. Géotechnique 34(4):449-489. https://doi.org/10.1680/geot.1984.34.4.449

119. Wu TH, Loh AK, Malvern LE (1963) Study of Failure Envelope of Soils. Journal of the Soil Mechanics and Foundations Division 89(1):145-181. https://doi.org/10.1061/JSFEAQ.0000481

120. Yamada Y, Ishihara K (1979) Anisotropic Deformation Characteristics of Sand under Three Dimensional Stress Conditions. Soils and Foundation 19(2):79-94. https://doi.org/10.3208/sandf1972.19.2_79

121. Zienkiewicz OC, Humpheson C, Lewis RW (1975) Associated and non-associated visco-plasticity and plasticity in soil mechanics. Géotechnique 25(4):671-689. https://doi.org/10.1680/geot.1975.25.4.671